Available online at www.sciencedirect.com
ScienceDirect
Palaeogeography, Palaeoclimatology, Palaeoecology 252 (2007) 304–327
PALAEO
www.elsevier.com/locate/palaeo

The Permian–Triassic boundary at Nhi Tao, Vietnam: Evidence for recurrent influx of sulfidic watermasses to a shallow-marine carbonate platform

Thomas J. Algeo [a,*], Brooks Ellwood [b], Thi Kim Thoa Nguyen [c], Harry Rowe [d], J. Barry Maynard [a]

[a] *Department of Geology, University of Cincinnati, Cincinnati, OH 45221-0013 USA*
[b] *Department of Geology and Geophysics, Louisiana State University, Baton Rouge, LA 70803, USA*
[c] *Institute of Geophysics, Vietnamese Academy of Science and Technology, Hanoi, Vietnam*
[d] *Department of Geological Sciences, University of Kentucky, Lexington, KY 40506, USA*

Accepted 30 November 2006

Abstract

The Permian–Triassic boundary at Nhi Tao, Cao Bang Province, Vietnam was sampled in a 7.5-m-thick outcrop section at high resolution (~5 cm intervals) for chemostratigraphic and magnetic susceptibility analysis. The section consists entirely of slightly argillaceous limestone representing shallow-marine facies of the Jinxi Platform, one of several large carbonate platforms within the Nanpanjiang Basin, located on the southern margin of the South China Craton. Upper Permian strata (Beds 1–7) are mainly dark-gray, cherty fossiliferous wackestones and packstones containing a diverse open-marine fauna, whereas uppermost Permian and Lower Triassic strata (Beds 9 and higher) are medium-gray calcimicrobial framestones containing rare macrofossils. These facies are separated by a 12-cm-thick oolitic–pisolitic grainstone (Bed 8) that coincides with the disappearance of most Late Permian faunal elements as well as with the first appearance of various geochemical anomalies that continue into the Lower Triassic part of the section. This "Late Permian event horizon" is characterized by (1) an abrupt decline in total organic carbon to near-zero values, (2) the onset of a sustained decline in carbonate δ^{13}C, and (3) the first of eight concentration peaks in pyrite sulfur. Significantly, each sulfide peak is associated with lower pyrite δ^{34}S values as well as with the *onset* of a negative carbonate δ^{13}C excursion (or the acceleration of an excursion already in progress). These chemostratigraphic relationships are consistent with multiple episodes of upwelling of sulfidic, ^{34}S- and ^{13}C-depleted deep-ocean waters onto the Jinxi Platform. The first upwelling event was the most intense and caused a drastic reduction in primary productivity and the demise of the Late Permian fauna; subsequent episodes were less intense but may have contributed to a delay in recovery of Early Triassic marine ecosystems. A ten-fold increase in magnetic susceptibility in Bed 9 may record the influx of fine detrital particles following destruction of terrestrial ecosystems and massive soil erosion. The terrestrial signal of the end-Permian catastrophe thus follows the marine signal with a 12-cm lag, which may reflect the time-of-transit of soil-derived particles across the Nanpanjiang Basin, suggesting that the marine and terrestrial crises in the Nhi Tao region occurred more-or-less synchronously. These observations suggest a model in which renewal of

---

[*] Corresponding author.
E-mail addresses: Thomas.Algeo@uc.edu (T.J. Algeo), Ellwood@lsu.edu (B. Ellwood), nkthoa@fpt.vn (T.K.T. Nguyen), hrowe@uky.edu (H. Rowe), Barry.Maynard@uc.edu (J.B. Maynard).

doi:10.1016/j.palaeo.2006.11.055

global-ocean overturn followed a prolonged interval of deep-ocean stagnation during the Late Permian, with upwelling intensity modulated by short-term (~20 kyr) climate cyclicity.

Keywords: Paleoceanography; Event stratigraphy; Upwelling; Geochemistry; Total organic carbon; Major elements; Trace elements; C-isotopes; O-isotopes; Magnetic susceptibility

---

1. Introduction

The Permian–Triassic boundary (PTB) (251.4±0.3 Ma, Bowring et al., 1998; 252.6±0.2 Ma, Mundil et al., 2004) is characterized by far-reaching changes in global climate, ecosystems, and geochemical cycles. The Late Permian mass extinction, which eliminated ~90% of marine and ~70% of terrestrial species, was the single largest extinction event in the Phanerozoic record and was followed by the widespread appearance of “disaster taxa” (Fig. 1; Raup, 1979; Schubert and Bottjer, 1992; Erwin, 1994; Retallack, 1995; Sepkoski, 1996; Baud et al., 1997; Rampino and Adler, 1998; Bowring et al., 1999; Jin et al., 2000; Benton and Twitchett, 2003). This event was associated with the onset of a pronounced negative shift (from −3 to −8‰) in marine carbonate δ^{13}C values (Baud et al., 1989; Holser et al., 1991; Baud et al., 1996; Jin et al., 2000; Cao et al., 2002; Korte et al., 2004; Payne et al., 2004; Horacek et al., 2007-this volume-a-b) and a correlative excursion in the organic carbon δ^{13}C records of both marine and terrestrial successions (Fig. 1; Hansen et al., 2000; Krull and Retallack, 2000; Krull et al., 2000; Twitchett et al., 2001; de Wit et al., 2002; Sephton et al., 2002). Further, various types of evidence (e.g., redeposited soils, influx of soil-derived organics to marine environments, and changes in stream morphology) have been interpreted to indicate widespread deforestation of land areas and rapid erosion of destabilized soils following the Late Permian mass extinction event (Sephton et al., 2005; Wang and Visscher, 2007-this volume).

Collectively, these observations suggest that the Late Permian event horizon (LPEH) was produced by a major catastrophic event, for which various mechanisms have been proposed (see reviews in Ward, 2000; Erwin et al., 2002; Berner, 2002; Benton, 2003). A case for a bolide impact was built on the basis of extraterrestrial He ratios,

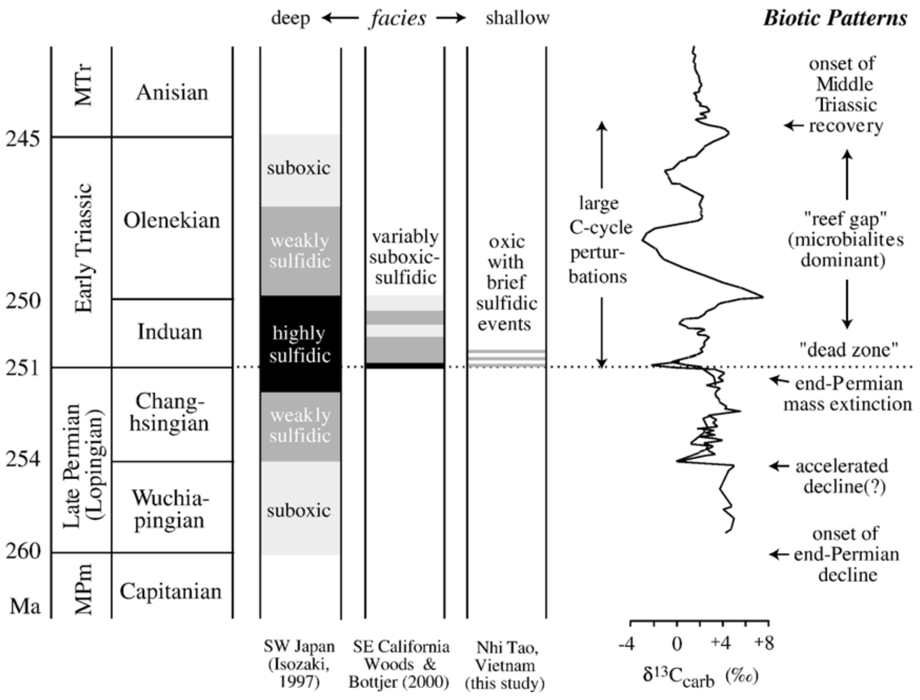

Fig. 1. Generalized depth-dependent redox conditions in Permian–Triassic oceans; based on Isozaki (1997), Woods and Bottjer (2000), and this study. Carbonate δ^{13}C data are for South China sections from Chen et al. (1991), Shao et al. (2000), and Payne et al. (2004). Biotic patterns summarized from Erwin (1994), Erwin et al. (2002) and other sources. Time scale is from Gradstein et al. (2004).

shocked quartz, and the identification of a potential impact crater on the northwest Australian continental margin (Gorter, 1996; Retallack et al., 1998; Becker et al., 2001; Basu et al., 2003; Becker et al., 2004), but all of these claims have been contested (Farley and Mukhopadhyay, 2001; Isozaki, 2001; Koeberl et al., 2002, 2004; Mundil et al., 2004; Müller et al., 2005). An alternative hypothesis invokes the eruption of the Siberian Traps flood basalts, the onset of which at 251.8 Ma is indistinguishable from the age of the LPEH (Renne and Basu, 1991; Campbell et al., 1992; Basu et al., 1995; Renne et al., 1995; Reichow et al., 2002; Kamo et al., 2003). This mechanism potentially triggered a variety of secondary effects disrupting global climate and ecosystems, e.g., massive discharge of dust and aerosols to the atmosphere leading to intense short-term climatic cooling (the so-called volcanic "nuclear winter" scenario), eustatic fall and catastrophic release of seafloor methane clathrates, longer-term climatic warming caused by a combination of volcanic CO_2 emissions and methane oxidation, and fallout of sulfate aerosols and acidification of land areas and, possibly, ocean-surface waters (Krull et al., 2000; De Wit et al., 2002; Fraiser and Bottjer, 2007-this volume).

Although a catastrophic event of some type appears to have occurred at the PTB, long-term changes in environmental conditions appear to have played a role as well. There is strong evidence for gradual environmental deterioration throughout the Late Permian, which may have stressed marine and terrestrial ecosystems prior to the main extinction event, as well as for persistence of inhospitable environmental conditions throughout the Early Triassic, which may have delayed the recovery of post-extinction biotas (Erwin, 1994; Stanley and Yang, 1994; Knoll et al., 1996; Retallack et al., 1996; Looy et al., 2001; Erwin et al., 2002; Wignall and Twitchett, 2002; Wignall and Newton, 2003; Huey and Ward, 2005; Isozaki et al., 2007-this volume). The accumulation of thick black shale successions in deepwater settings has been cited as evidence of long-term (>10 Myr) deep-ocean anoxia during the Permian–Triassic transition (Fig. 1; Wignall and Hallam, 1992; Isozaki, 1997; Suzuki et al., 1998; Hotinski et al., 2001; Zhang et al., 2001; Kato et al., 2002; Wignall and Twitchett, 2002). Paleoceanographic modeling of Late Permian oceans suggests that sluggish circulation was a likely consequence of changes in the hydrologic cycle, the locus of deepwater formation, and the pole-to-equator temperature gradient (Hotinski et al., 2001; Zhang et al., 2001; Kiehl and Shields, 2005; Winguth and Maier-Reimer, 2005). Prolonged stagnation and deeper penetration of organic detritus as a result of enhanced ballasting resulted in deep-ocean waters that were strongly oxygen deficient and sulfidic. Subsequent reinvigoration of global-ocean overturn would have transferred these toxic waters to shallow-marine environments, with lethal effects for many shallow-marine organisms (Kajiwara et al., 1994; Grice et al., 2005; Winguth and Maier-Reimer, 2005). A related mechanism is upward chemocline excursion, in which the O_2–H_2S boundary gradually rose into ocean-surface waters as a consequence of stagnant circulation and, possibly, low atmospheric O_2 levels (Kump et al., 2005). One or both of these mechanisms could account for reports of episodic anoxia in Early Triassic platform facies as well as for the delayed recovery of Early Triassic marine ecosystems (Wignall and Hallam, 1992; Woods et al., 1999; Woods and Bottjer, 2000; Fig. 1).

In the present study, we investigate proxies for chemical oceanographic changes within a PTB section at Nhi Tao, Vietnam. One important feature of the study section is that its bulk lithology, weakly argillaceous limestone, is virtually unchanged through the PTB interval (although a change in microfacies does occur; see Section 2). This is a favorable circumstance for evaluation of hydrogenous (seawater-sourced) chemostratigraphic signals, which tend to be obscured in lithologically heterogeneous sections (e.g., Yang et al., 1995; Yin et al., 2001; Algeo et al., 2007-this volume). Although nearly uniform carbonate successions are known from other PTB locales worldwide (e.g., Holser et al., 1991; Lehrmann et al., 2001, 2003; Heydari et al., 2003; Korte et al., 2004; Krull et al., 2004; Lehrmann et al., 2005; Baud et al., 2005), few if any of these sections have been sampled at the level of resolution or subjected to the integrated suite of geochemical analyses applied in the present study. The present high-resolution analysis of the Nhi Tao section using multiple chemostratigraphic proxies provides evidence of large, high-frequency changes in seawater chemistry during the latest Permian and Early Triassic, and the significance of these changes for understanding the origin of the PTB will be considered in this contribution.

2. Geologic background

The study section is situated near the cistern of Nhi Tao village, 13 km northwest of the town of Tra Linh, in Cao Bang province, Vietnam (Fig. 2A; Doan et al., 2004; Nguyen et al., 2004). During the Late Permian and Early Triassic, this area was part of the South China (or Yangtze) Craton, which was located near the paleoequator in the eastern half of the Paleotethys Ocean (Fig. 2B). This craton was one of a number of small continental and volcanic arc

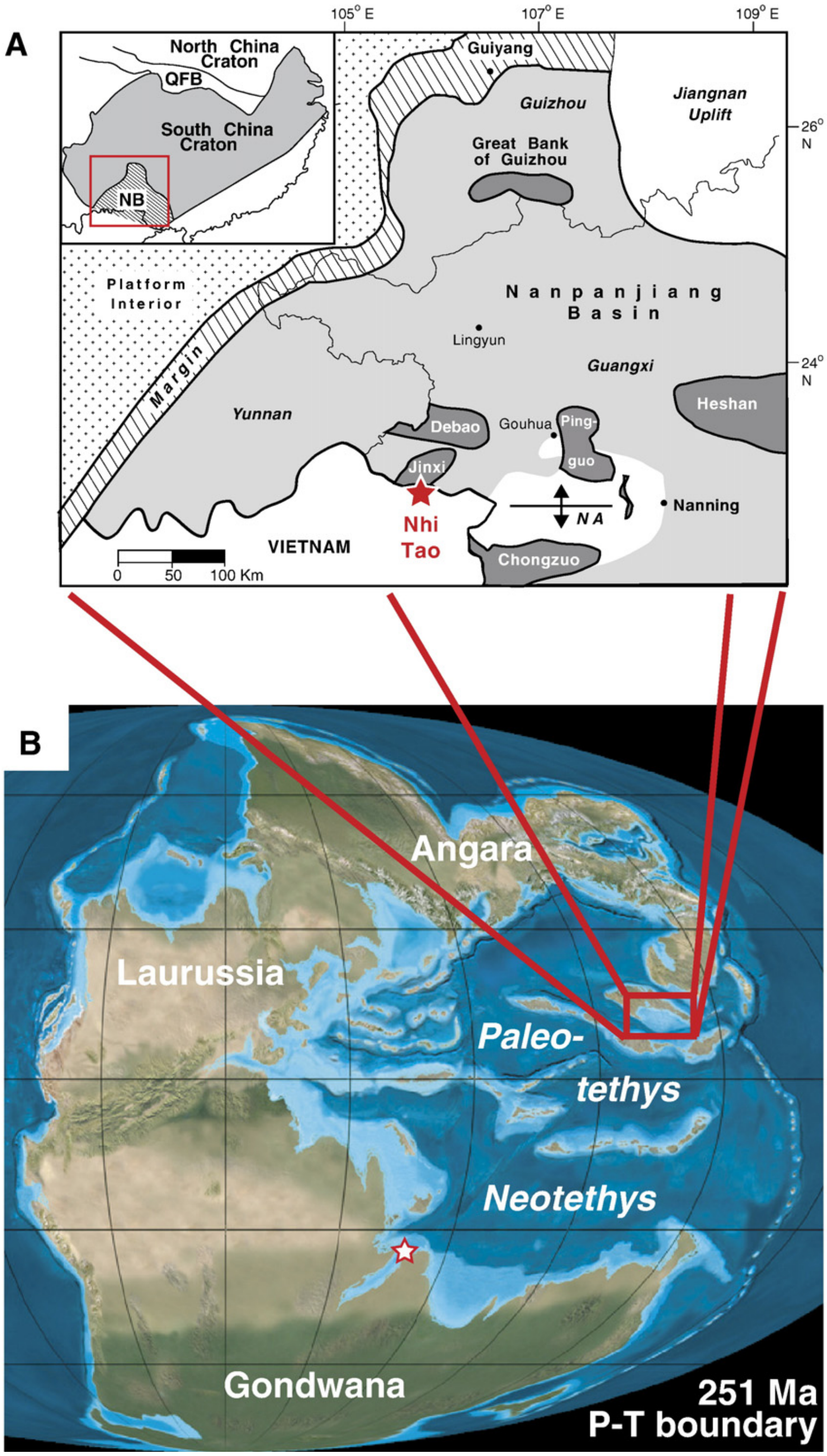

Fig. 2. (A) Regional paleogeography and location map for the Nhi Tao PTB section; note proximity of section to the Vietnam–China border. The Jinxi Platform was one of several carbonate platforms developed within the Nanpanjiang Basin, on the southern margin of the Late Permian South China Craton. NA = Nanning Anticline, NB = Nanpanjiang Basin, QFB = Qinling Fold Belt. Modified from Lehrmann et al. (2001, 2003, 2007-this volume). (B) Permian–Triassic boundary global paleogeography. The star on the northern Gondwana margin shows the location of the Guryul Ravine section (see Algeo et al., 2007-this volume). Base map courtesy of Ron Blakey (http://jan.ucc.nau.edu/~rcb7/).

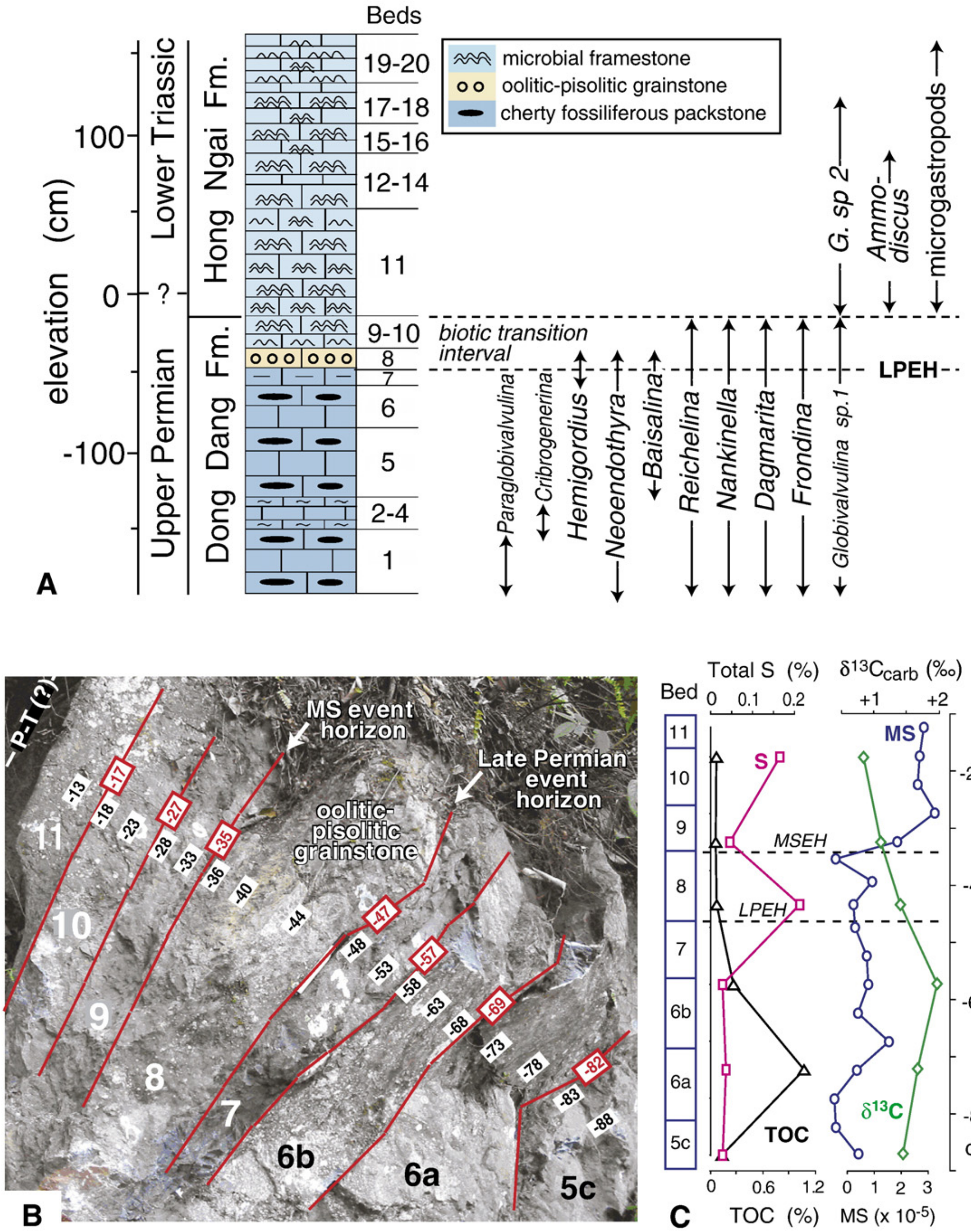

Fig. 3. (A) Biostratigraphy of the Nhi Tao section (from Nguyen et al. (2004), and Nguyen Thi Kim Thoa, unpubl. data). The "biotic transition interval" corresponding to Beds 8 to10 marks holdover of some Late Permian faunal elements in much reduced abundances. (B) Outcrop photo of Beds 5c to 11, representing the latest Permian interval. Inclined numbers give stratigraphic position relative to the PTB in centimeters; red = bed contacts, black = sample levels. Apparent nonuniformity of scale across the center of photo is an optical illusion produced by the nonplanar surface of the outcrop. The inferred position of the PTB is within Bed 11, on the left margin of the photo. (C) Detail of the chemostratigraphy of Beds 5c to 11. The Late Permian event horizon (LPEH) coincides with the base of Bed 8 and the main excursion in the MS record is at the base of Bed 9.

terranes that were beginning to assemble to form present-day eastern Asia, a process that was largely completed during the Triassic Indosinian Orogeny (Lepvrier et al., 2004). Whereas much of the South China Craton was subaerially exposed or shallowly flooded, its southern margin was occupied by the deepwater Nanpanjiang Basin. This basin contained a number of large (>50 km wide) carbonate platforms on which accumulated shallowsubtidal and peritidal sediments (Lehrmann, 1999; Lehrmann et al., 2001, 2003, 2005, 2007-this volume). The Nhi Tao section was located on the southeastern margin of the Jinxi Platform, which straddles the present-day Vietnam–China border (Fig. 2A).

The Nhi Tao PTB section is 7.5 m thick and consists of slightly argillaceous limestone (Fig. 3A–B; Doan et al., 2004; Nguyen et al., 2004). Upper Permian strata (Beds 1–7) are medium gray and contain abundant dark-gray chert nodules; the dominant microfacies is a skeletal packstone containing a diverse, open-marine fauna, including many species of benthic foraminifera. Bed 8, representing the Late Permian event horizon (LPEH) at which most Late Permian faunal elements went extinct, is a 12-cm-thick oolitic–pisolitic grainstone that coincides with the last appearance of the benthic foraminifera *Hemigordius*, *Neoendothyra*, *Baisalina* (Fig. 3A). The overlying uppermost Permian and Lower Triassic strata (Beds 9 and higher) consist largely of light-gray calcimicrobial (*Renalcis*-type) framestones with rare fossiliferous interbeds. Beds 9 and 10 contain scattered tests of the benthic foraminifera *Reichelina*, *Nankinella*, *Dagmarita*, *Frondina*, and *Globivalvulina* sp. 1 that may represent taphonomically reworked shells or, alternatively, short-term survivors of the environmental changes associated with the LPEH. In Bed 11 and higher, new members of a depauperate Early Triassic biota are found, including microgastropods and the foraminifers *Ammodiscus planus*, *A. parapriscus*, and *Globivalvulina* sp. 2 (Fig. 3A).

Biostratigraphic identification of the PTB in the Nhi Tao section is tentative, in part because no conodont or palynological studies have been published to date. The first appearance of the conodont *Hindeodus parvus* (Kozur et Pjatakova) in the Permian–Triassic global stratotype section and point (GSSP) at Meishan D (Changhsing district, Zhejiang Province, China) is now recognized as the marker for the base of the Triassic System (Yang et al., 1995; Yin et al., 2001). Elsewhere, the PTB is considered to be the equivalent time-stratigraphic horizon, but the regionally diachronous first appearance of *H. parvus* commonly creates difficulties in narrowly locating the PTB in other sections. At Nhi Tao, *H. parvus* has been identified in a limestone bed about 7 m above Bed 20 (Doan et al., 2004), but this is unlikely to be correlative with its first appearance at Meishan D. The Nhi Tao section contains a low-abundance “transitional” fauna in Beds 9 and 10 and a more characteristically Early Triassic fauna in Beds 11 and higher (Fig. 3A), suggesting that the PTB is present within Bed 11, about 40 to 50 cm above the LPEH (=Bed 8).

3. Methods

Whole-rock major- and trace-element concentrations were determined using a wavelength-dispersive Rigaku 3040 XRF spectrometer at the University of Cincinnati. Results were calibrated using both USGS and internal laboratory standards. A suite of carbonate and marl laboratory standards was generated for this study, the compositions of which were determined by XRAL Incorporated through XRF and INAA. Analytical precision based on replicate analyses was better than ±2% for major and minor elements and ±5% for trace elements. Detection limits were ~5 ppm for most trace elements. Carbon and sulfur elemental concentrations were measured using an Eltra 2000 C–S analyzer. Data quality was monitored via multiple analyses of the USGS SDO-1 standard (TC = 9.68 wt.%; TS = 5.35 wt.%) and a pure $CaCO_3$ standard (TC = 12.00 wt.%), with an analytical precision (2σ) of ±2.5% of reported values for carbon and ±5% for sulfur. An aliquot of each sample was digested in 2 N HCl at 50 °C for 12 h to dissolve carbonate minerals, and the residue was analyzed for total organic carbon (TOC) and non-acid-volatile sulfur (NAVS); total inorganic carbon (TIC) and acid-volatile sulfur (AVS) were obtained by difference.

XRD analysis showed that illite, dolomite, and calcite were the only quantitatively important minerals present in the study samples. The fractions of these minerals in each sample, as shown in Fig. 4, were estimated as follows:

$$\text{Illite} = \text{Al}/\text{Al}_{\text{illite}} \tag{1}$$

$$\text{Dolomite} = [(\text{Mg}-\text{Mg}_{\text{detr}})\,\text{x}\,24.0/24.3]/\text{TIC}\,\text{x}\,(1-\text{Illite}) \tag{2}$$

$$\text{Calcite} = [(\text{Ca}-\text{Ca}_{\text{detr}})\ \text{x}\ 12.0/40.1]/\text{TIC}\ \text{x}\ (1-\text{Illite}) \tag{3}$$

Because illite is the major Al-bearing mineral in the study section, its fraction (Eq. (1)) can be calculated as the ratio of sample Al to the average Al concentration of pure illite (~13%; Grim, 1968). The dolomite and calcite fractions (Eqs. (2) and (3)) are calculated as the weight ratio of dolomite or calcite C (bracketed subequations) to total inorganic carbon (TIC) for the carbonate fraction of the sample (1 — Illite). Dolomite (calcite) C is calculated as percent nondetrital Mg (Ca) multiplied by the molar weight ratio of C to Mg (Ca) in dolomite (calcite), i.e., 24.0/24.3 and 12.0/40.1, respectively. Detrital magnesium and calcium, Mg_{detr} and Ca_{detr}, are calculated as the average Mg and Ca

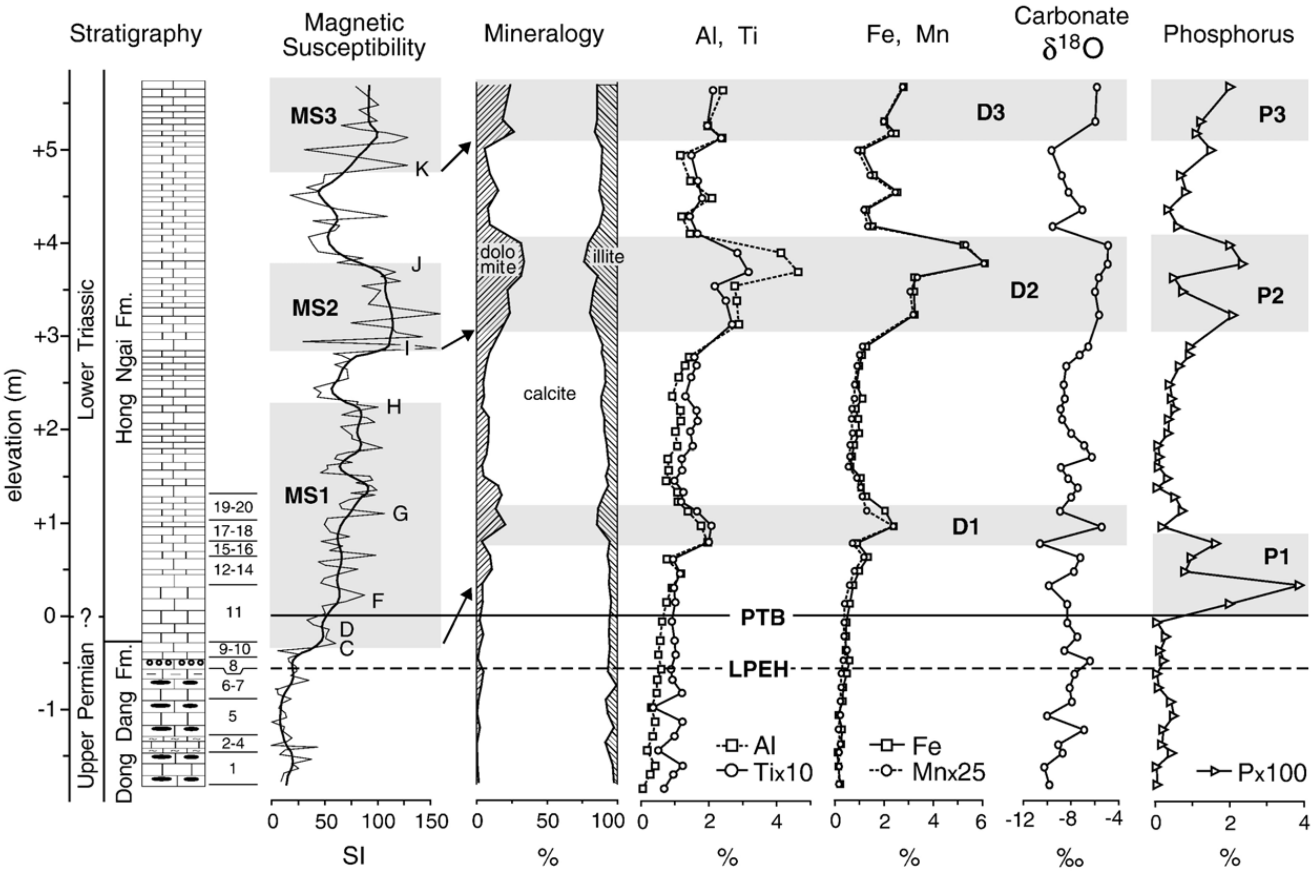

Fig. 4. Stratigraphic trends in magnetic susceptibility, mineralogy, carbonate δ^{18}O, and P. Shaded fields MS1 to MS3 represent intervals of high or rising MS values; D1 to D3 represent more dolomitic and detrital-rich portions of the section; P1 to P3 represent phosphorus-enriched intervals. On the magnetic susceptibility curve, C to K represent features used in correlation of the Nhi Tao section with the Meishan D MS record (Figs. 7 and 8). For calculation of percent dolomite, calcite, and illite, see Eqs. (1)–(3) of text. LPEH = Late Permian event horizon; PTB = Permian–Triassic boundary.

concentrations of pure illite (~2.1% and 0.5%, respectively; Grim, 1968) multiplied by Al/$\text{Al}_{\text{illite}}$, the ratio of sample Al to average illite Al. The sum of the three fractions above yielded a mean of 101.5 ± 6.3 % for the 44 study samples as a group, validating the utility of the procedure above for quantitative estimation of mineral fractions in the study unit. For each sample, the sum of the three fractions was normalized to 100% for graphic display (Fig. 4).

Stable C and O isotopic compositions of carbonates were analyzed at the University of Kentucky Environmental Research Training Laboratory using a GasBench—II peripheral coupled to a Delta*Plus*XP isotope ratio mass spectrometer. Samples (450 ± 50 μg) were equilibrated at 40 °C for 24 h before analysis. Average precision for δ^{13}C and δ^{18}O of NBS-19 calcite standard was 0.05‰ and 0.05‰, respectively, for the entire dataset. Average precision for δ^{13}C and δ^{18}O of unknowns was 0.02‰ and 0.05‰, respectively. All results are reported relative to V-PDB.

The limestones examined in this study are dominated by diamagnetic phases exhibiting weak magnetic susceptibility (MS). Measurement of MS in such samples requires greater sensitivity than provided by most commercially available instruments. All measurements reported in this paper were performed using a high-sensitivity susceptibility bridge at Louisiana State University (LSU). Instrument calibration uses standard salts for which values were reported in Swartzendruber (1992) and the Handbook of Physics and Chemistry (2004); it is also cross-calibrated against a KLY-3S Kappa Bridge at LSU. Each sample was measured three times, and the mean of these measurements is reported. MS values were initially determined in units of $m^3\ kg^{-1}$ but have been recalculated in SI units here for purposes of comparison with MS data from Meishan D (Hansen et al., 2000). This introduces some error owing to use of an assumed sample density (2700 kg m^{-3}), but it is not likely to significantly affect the MS chemostratigraphic trends or comparisons between sections reported in this study.

4. Results

4.1. Chemostratigraphy of the Nhi Tao PTB section

The bulk lithology of the Nhi Tao PTB section is slightly argillaceous limestone. The carbonate fraction, mostly composed of calcite, is consistently >75% of sample weight and averages ~90% for the section as a whole (Fig. 4). Dolomite abundance is negligible in the Upper Permian but increases somewhat in the Lower Triassic, with local concentrations associated with detrital horizons D1–D3 (Fig. 4). Although no primary aragonite remains, moderately elevated Sr concentrations in Upper Permian Beds 1–7 (to 2000 ppm; not shown) suggest the former presence of aragonitic fossils or cements comprising ~5 to 25% of the sediment mass. In contrast, uppermost Permian and overlying Lower Triassic strata (Beds 8 and higher) exhibit uniformly low Sr concentrations (300±50 ppm), consistent with a lack of primary aragonitic skeletal debris and dominance of a LMC-secreting microbial biota following the Late Permian mass extinction.

The non-carbonate fraction consists mainly of clay minerals (with minor authigenic chert in Upper Permian Beds 1–7), averaging ~10% of sample weight for the section as a whole. Vertical trends in clay mineral content can be evaluated from detrital-fraction proxies, e.g., Al and Ti (Fig. 4). There is a gradual increase upsection in the clay fraction commencing ~50 cm above the PTB, punctuated by local concentrations at three stratigraphic levels (detrital horizons D1–D3). These horizons are also associated with increases in Fe and Mn concentrations (Fig. 4), although it is uncertain whether the latter are present as minor constituents of ferrous dolomite, as structural components of clay minerals, or as adsorbed phases on detrital-particle surfaces. The close association of dolomite with the detrital fraction suggests that the dolomitization process was catalyzed by clay minerals, owing either to increased availability of Mg or to control of porefluid mobility. In either case, dolomitization is likely to have occurred in the burial diagenetic environment. Phosphorus also generally exhibits a close association with the detrital fraction (e.g., horizons P2 and P3 correlate with D2 and D3; Fig. 4), although the largest P peak (P1) is not associated with a shaly interval; its significance will be considered below.

Carbonate δ^{18}O values are moderately variable, ranging from −4.9 to −10.6‰ (Fig. 4). There is a slight upsection trend toward more ^{18}O-enriched values, but, in view of the limited thickness (7.5 m) of the section, this cannot reflect variation in burial temperatures. Rather, the most likely control on carbonate δ^{18}O values is the proportion of dolomite, as the dolomitic horizons (D1–D3; Fig. 4) exhibit distinct ^{18}O enrichment relative to adjacent, more purely calcitic horizons. This pattern may reflect the known ~3‰ ^{18}O enrichment of dolomite precipitated in thermodynamic equilibrium with calcite (Vasconcelos et al., 2005). About half of the variance in the carbonate δ^{18}O record can be attributed to variations in dolomite abundance, with the other half possibly related to variations in primary porosity or grain size that influenced the timing of burial diagenetic stabilization. The relationship between carbonate δ^{18}O values and dolomite abundance is consistent with the inference that dolomitization was a burial diagenetic process.

Whereas the proxies considered above reflect the bulk geochemistry of the study section, a separate group of proxies consisting of TOC, trace metals, carbonate δ^{13}C, and sulfur provide information about minor sedimentary constituents. Although total organic carbon (TOC) is in limited abundance throughout the Nhi Tao section, Upper Permian Beds 1–7 contain measurable quantities (>0.5%; Figs. 3C, 5) in comparison with the near-zero concentrations (<0.1%) found in uppermost Permian and Lower Triassic Beds 8 and higher. The abrupt decline in TOC is correlative with the LPEH and the microfacies transition from fossiliferous packstones to calcimicrobial framestones. Redox-sensitive trace metals (e.g., Mo, U and V) exhibit stratigraphic trends that parallel TOC, i.e., modest enrichment in Beds 1–7 and negligible concentrations higher in the section (Fig. 5). Limited uptake of trace metals by the sediment may indicate generally oxic environmental conditions or, alternatively, simply a lack of organic-matter host substrates for trace-metal adsorption. The latter explanation may be more likely because (1) small enrichments of V are associated with some of the sulfidic event horizons (e.g., S6 and S8; Fig. 5), and V (unlike Mo and U) does not necessarily require an organic host substrate (Algeo and Maynard, 2004), and (2) there is independent evidence for episodically sulfidic conditions at Nhi Tao during the latest Permian–Early Triassic (see Discussion below).

The carbonate δ^{13}C record exhibits a highly distinctive pattern of chemostratigraphic variation (Figs. 3C, 5). Upper Permian Beds 1–7 are relatively ^{13}C-enriched, fluctuating between +1.2 and +2.6‰. The overlying uppermost Permian strata (Beds 8–11) record a rapid, monotonic shift toward more ^{13}C-depleted values, from +2.2 at the LPEH to 0‰ just above the PTB (Fig. 5). Above the PTB, the carbonate δ^{13}C record exhibits quasi-cyclic fluctuations between ca.−1.0 and 0‰ at a length scale of ~50 to 150 cm, with only a small (ca.−0.5‰) shift in average δ^{13}C values through the ~6-m-thick Lower

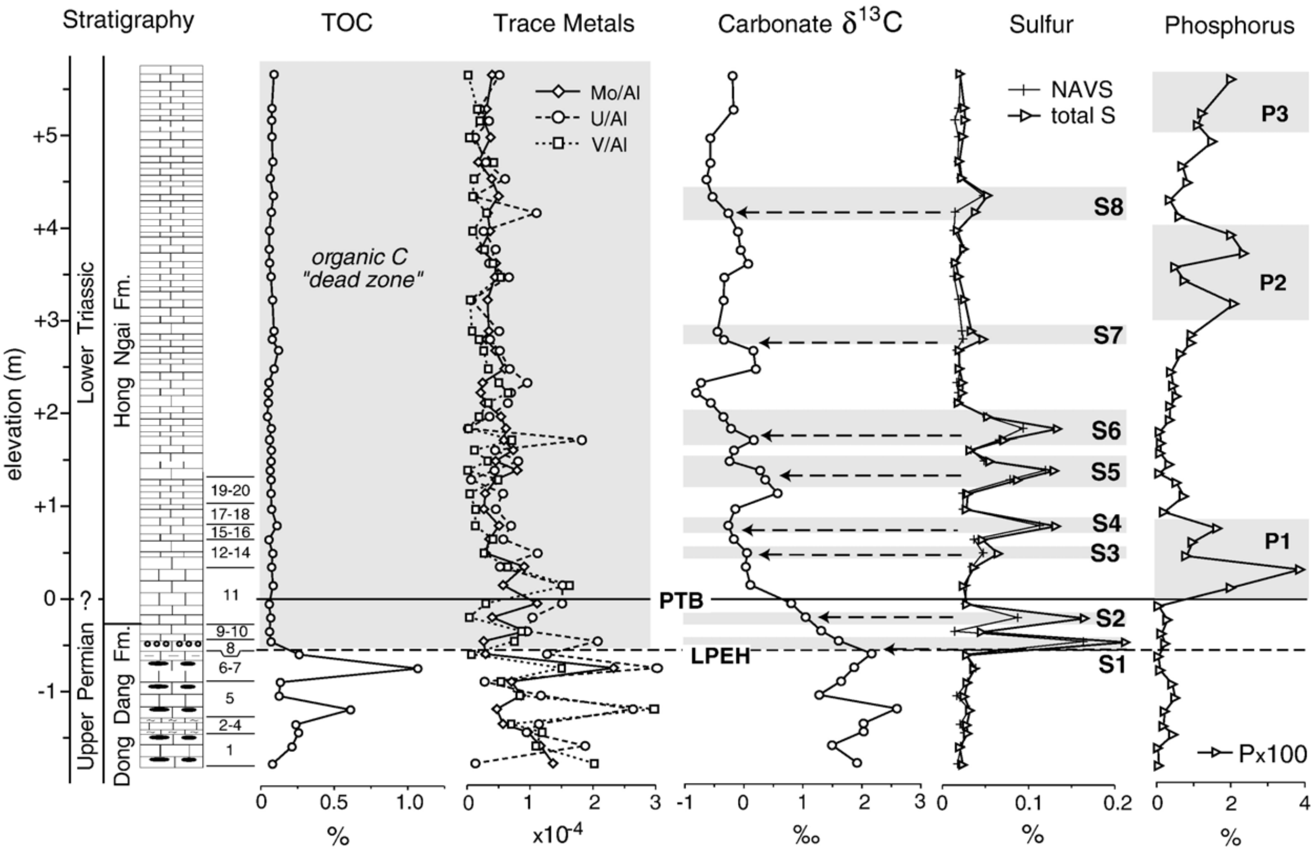

Fig. 5. Stratigraphic trends in minor-fraction elemental proxies, carbonate δ^{13}C, and P. The total and pyrite [S] records exhibit eight maxima (S1 to S8), each of which except S4 correlates with the *onset* of a negative excursion in the carbonate δ^{13}C record (or with intensification of an excursion in progress, as for S2). NAVS = non-acid-volatile sulfur. LPEH = Late Permian event horizon; PTB = Permian–Triassic boundary.

Triassic interval. Carbonate δ^{13}C values exhibit no covariation with carbonate δ^{18}O either below or above the PTB (Fig. 6; cf. Korte et al., 2004), nor do they show any relationship to bulk lithology (Fig. 4). These observations are consistent with interpretation of the carbonate C-isotopic record as a primary depositional signal (i.e., largely unaltered marine carbonate δ^{13}C values).

Sulfur concentrations, although small in absolute terms (0.10–0.22 wt.%), exhibit significant chemostratigraphic variation (Fig. 5). Both total and pyrite [S] are uniformly low (<0.05%) in Upper Permian Beds 1–7 but increase abruptly to >0.2% at the LPEH and then rise episodically to >0.1% in Lower Triassic strata. Eight distinct sulfide peaks are observed (horizons S1–S8), with a general upsection trend toward lower maximum values. Although complete sulfur speciation has not been undertaken, the main host phase for sulfur is likely to be pyrite: (1) organic matter is virtually absent in uppermost Permian and Lower Triassic strata (Fig. 5), implying a lack of organic sulfur, (2) non-acid-volatile sulfur (NAVS) comprises the bulk of total S (Fig. 5), suggesting a lack of Fe-monosulfides and carbonate-associated sulfate, and (3) although the Nhi Tao samples were too small for both thin-section and geochemical analysis, petrographic study of a PTB section at Dawen, China (about 350 km to the northeast) revealed the presence of numerous clusters of small (<10 μ) pyrite framboids in samples taken from above the LPEH (Algeo, unpubl. data). A significant observation is the close

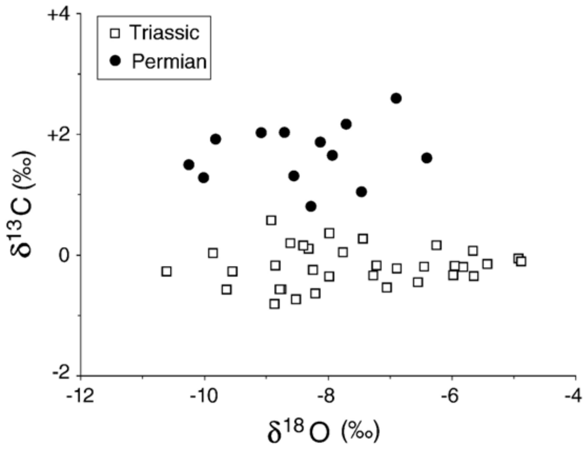

Fig. 6. C–O isotopic crossplot. All values are relative to the V-PDB standard. Lack of any correlation between δ^{13}C and δ^{18}O values is consistent with the inference that the C-isotope record in the Nhi Tao section is primary (i.e., largely unaltered marine values).

relationship between sulfide peaks and the *onset* of negative excursions in the carbonate δ^{13}C record (dashed arrows, Fig. 5; see Discussion below).

4.2. Correlation with the Meishan D Permian–Triassic boundary GSSP

The Nhi Tao PTB section can be correlated with the Meishan D GSSP on the basis of a combination of carbonate δ^{13}C and MS chemostratigraphy, event beds, and biostratigraphy. At Meishan, the carbonate δ^{13}C record records a ca. −3‰ shift at the top of bed 24e (Xu and Yan, 1993; Jin et al., 2000), representing the negative excursion found in latest Permian strata at many locales globally (Corsetti et al., 2005). The sharpness of this shift at Meishan could be interpreted as evidence of a disconformity at this level (cf. Wang et al., 1994), but the overall correlation framework between Meishan and Nhi Tao (Fig. 7) suggests that little, if any, time is missing. Rather, the Meishan carbonate δ^{13}C record appears to be problematic: (1) significant differences exist between the closely spaced Meishan B and D sections, and (2) neither Meishan section exhibits a gradual excursion across the PTB toward more ^{13}C-depleted values, as commonly seen in high-resolution records elsewhere (e.g., Holser et al., 1991; Baud et al., 1996; this study). Nonetheless, the sharp C-isotopic shift at the top of bed 24e at Meishan appears to be correlative with the onset of a protracted negative C-isotopic excursion in Bed 8 at Nhi Tao (datum B; Fig. 7). Below datum B, a smaller, transient excursion toward more ^{13}C-depleted values near the base of bed 24e at Meishan and within Bed 5 at Nhi Tao also may be correlative (datum A; Fig. 7). Above datum B, the C-isotopic records of the Meishan D and Nhi Tao PTB sections bear little similarity. The anomalous

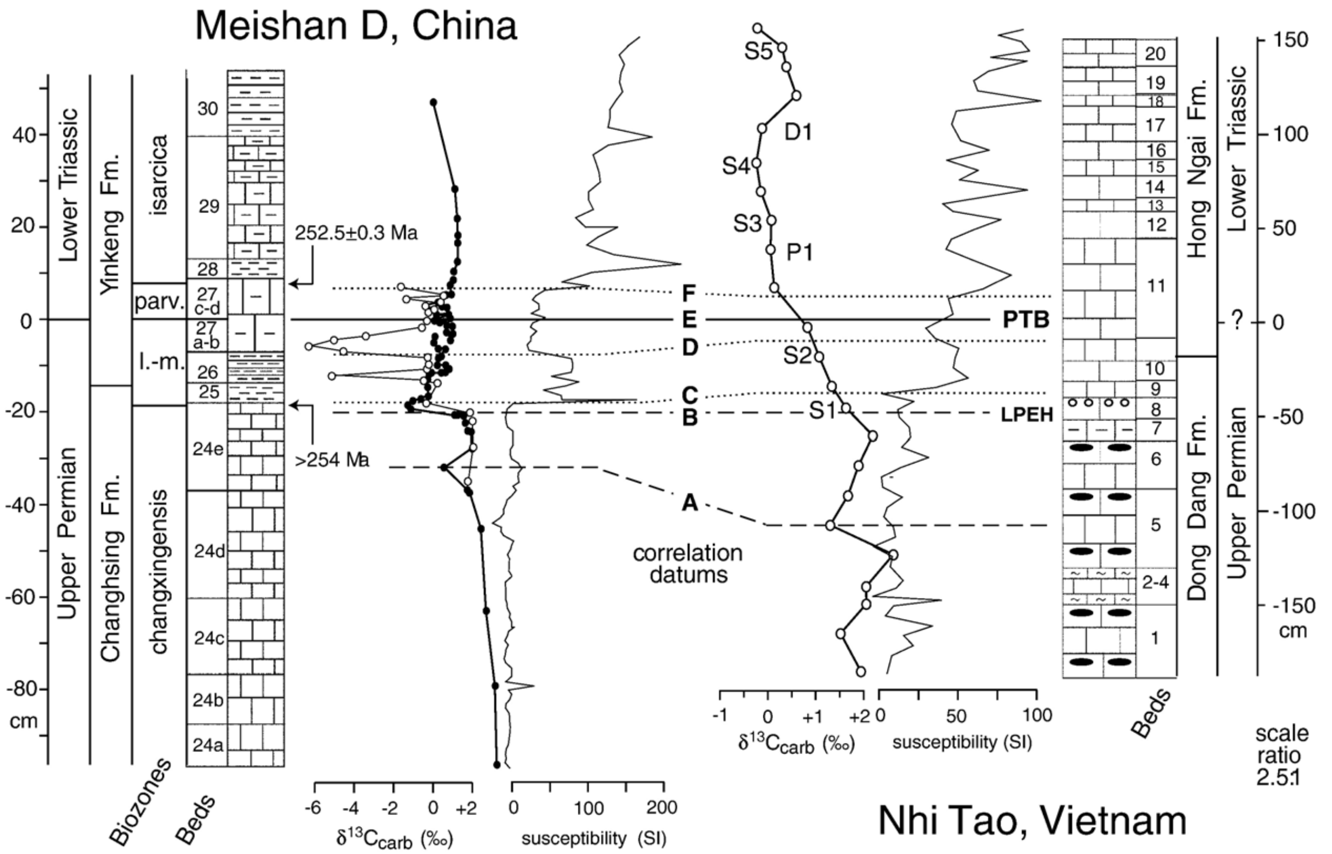

Fig. 7. Correlation of Nhi Tao (Vietnam) and Meishan D (China) Permian–Triassic boundary sections. The stratigraphic column for Meishan D is from Jin et al. (2000), conodont biozones from Yin et al. (2001), radiometric ages from Mundil et al. (2001), and MS data from Hansen et al. (2000). Carbonate δ^{13}C records for Meishan D and B are from Xu and Yan (1993; open circle) and Jin et al. (2000; solid circle), respectively. The two large negative excursions in beds 26 and 27 of the Xu and Yan curve are likely to be artifacts associated with low carbonate content (Bachmann and Kozur, 2004); the Jin et al. curve was confirmed by Cao et al. (2002). Correlation datums A to F levels are based on matching features of the carbonate δ^{13}C (dashed lines) or MS records (dotted lines); datum E is the Permian–Triassic boundary. The stratigraphic position of sulfur (S1–S5), phosphorus (P1), and dolomite (D1) anomalies from Figs. 4 and 5) are shown relative to the carbonate δ^{13}C curve. The scale ratio between the Nhi Tao and Meishan D sections, 2.5:1, is approximately the ratio of sedimentation rates between these sections in stratigraphic proximity to the PTB. LPEH = Late Permian event horizon; PTB = Permian–Triassic boundary.

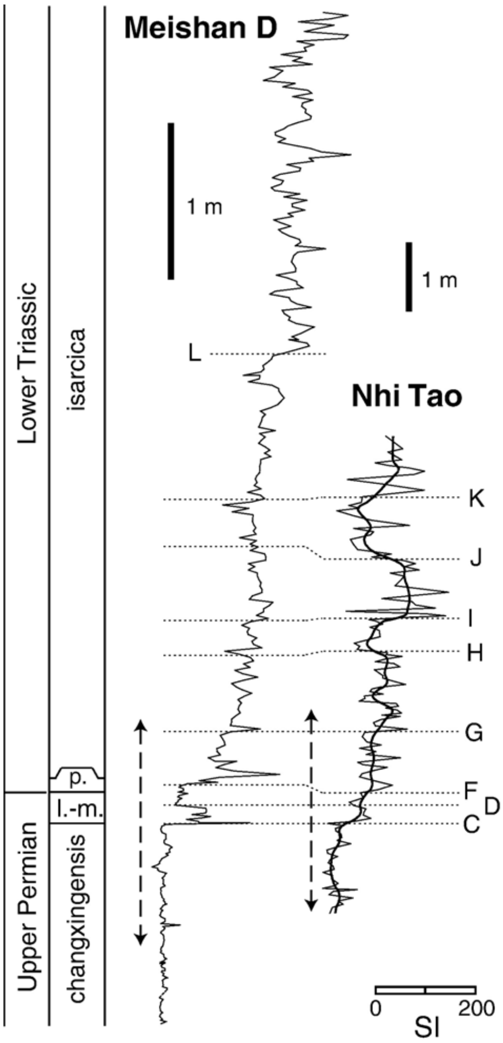

Fig. 8. Complete MS record of the Nhi Tao section, compared with the stratigraphically equivalent interval at Meishan D. Both records exhibit a sharp rise from MS values <25 SI in the Late Permian to ~150–200 SI in the Early Triassic. Within this interval, a series of characteristic features (C to K) can be correlated between the two sections. At Meishan D, a sharp shift to a higher plateau (~300 SI; feature L) is observed further upsection; the Nhi Tao record does not extend to this stratigraphic level, indicating that the latter section comprises only the lowermost ~25% of the *isarcica* zone. Data for Meishan D are from Hansen et al. (2000). Abbreviations: l.-m. = *latidentatus–meishanensis* zone, p. = *parvus* zone. Vertical dashed arrows represent the portions of the MS records that are shown in Fig. 7.

character of the Meishan C-isotopic records is likely to be due to analysis of carbonate-poor clays, in which impurities can markedly influence the signal (Bachmann and Kozur, 2004).

In contrast to the carbonate δ^{13}C records, the MS records of the Meishan D and Nhi Tao sections exhibit striking similarities from which multiple correlation datums (C to K) can be generated (Figs. 7 and 8). Both sections exhibit low MS values (<25 SI) below the LPEH. Slightly above the LPEH (5 cm at Meishan, 15 cm at Nhi Tao), there is a sharp increase in MS values above the Upper Permian baseline (datum C). From this point, there is a general upsection increase in MS values, culminating in a plateau with values of 150–200 SI between datums I and J (Fig. 8). At Meishan D, there is a second shift to an even higher MS baseline (250–300 SI) above datum L, but the correlative portion of the Nhi Tao section has not been sampled.

The detailed correlation framework between Meishan D and Nhi Tao (Figs. 7 and 8) permits several inferences. First, within the resolution limits of this framework, the LPEH (datum B) and the PTB (datum E) were synchronous events at Meishan and Nhi Tao. Although not unexpected, this observation provides general validation of the correlation framework as well as support for the tentative location of the PTB within Bed 11 at Nhi Tao (Fig. 3A; Nguyen et al., 2004). Second, the similar spacing of datums implies that sedimentation rates were fairly uniform in both sections, or that they varied largely in tandem. Third, based on the relative thicknesses of correlative intervals, average sedimentation rates at Nhi Tao were ~2.5 times greater than those at Meishan D. Only small variations in datum spacing exist, e.g., a slight condensation of the interval between datums A and D at Meishan relative to Nhi Tao. Fourth, the Nhi Tao section extends only through the lowermost ~25% of the *isarcica* zone, the complete thickness of which is ~10 m at Meishan D. The *isarcica* zone represents approximately 1/5 of the ~2-Myr-long Induan Stage, or ~400 kyr (Kozur, 2003), and the portion sampled at Nhi Tao thus represents ~100 kyr. Fifth, sedimentation rates at both Meishan and Nhi Tao appear to have been low within the PTB interval *sensu stricto* and to have accelerated during the Early Triassic. Based on radiometric dating and cyclostratigraphic analysis of the Meishan section, the 18-cm-thick interval of beds 25–27b (i.e., between the LPEH and PTB) was deposited at an average rate of ~1.5 mm kyr^{-1}, and the 10-m-thick interval of the *isarcica* zone (beds 28 and up) at an average rate of ~24 mm kyr^{-1} (Bowring et al., 1998; Kozur, 2003). Given the greater sedimentation rates at Nhi Tao (see above), the corresponding estimates are ~4.2 mm kyr^{-1} for Beds 9–11(lower half) and ~60 mm kyr^{-1} for Beds 11(upper half) and higher.

The probable stratigraphic completeness of the Nhi Tao section is suggested by the gradualness of changes in its carbonate δ^{13}C record (Fig. 7; cf. Holser et al., 1991; Kakuwa and Matsumoto, 2006). The comparatively high stratigraphic resolution afforded by this section is critical to delineation of closely spaced events within the PTB interval and, hence, to determination of cause-and-effect relationships among contemporaneous biotic, oceanographic, and climatic factors. PTB sections in eastern Greenland and Kashmir may afford even higher stratigraphic resolution (e.g., Looy et al., 2001; Twitchett et al., 2001; Brookfield et al., 2003; Algeo et al., 2007-this volume), but these are dominated by paralic siliciclastics that were not prone to recording the strong hydrogenous signal necessary for analysis of chemical paleoceanographic events. Other stratigraphically expanded marine PTB sections (e.g., Holser et al., 1991; Horacek et al., 2007-this volume-a-b) have not been the subject of comprehensive chemostratigraphic analyses to date. For these reasons, the results of the present study of the Nhi Tao section may assume a special importance for PTB research.

5. Discussion

5.1. The Late Permian event horizon (LPEH)

The Late Permian event horizon (LPEH), the stratigraphic level marking the abrupt disappearance of most Late Permian faunal elements and simultaneous appearance of various chemostratigraphic anomalies, is associated with a bed of highly distinctive petrographic character in the Nhi Tao PTB section. This bed (Bed 8) consists of oolitic–pisolitic grainstone, representing a transition between underlying cherty fossiliferous wackestone–packstones and overlying calcimicrobial framestones (Fig. 3). Visual inspection of the Bed 8 sample prior to grinding showed that it consisted almost entirely of large ooids and pisoids (diam. 2–8 mm) exhibiting moderate sorting. Abiotic carbonate grains and synsedimentary cements are common features of PTB sections deposited in shallow- to intermediate-depth marine environments, both at the boundary *sensu stricto* and in stratigraphically younger beds within the Lower Triassic (e.g., Holser et al., 1991; Wignall and Hallam, 1992; Grotzinger and Knoll, 1995; Woods et al., 1999; Lehrmann et al., 2001, 2003, 2005; Heydari et al., 2003; Baud et al., 2005; Lehrmann et al., 2007-this volume). Such deposits are commonly interpreted as event beds associated with major chemical oceanographic changes that led to an increase in the carbonate saturation of ocean-surface waters. Such changes can occur through mixing of watermasses of dissimilar chemistry, especially when the activities of key ionic species differ (Wigley and Plummer, 1976; Arp et al., 2003).

The LPEH coincides with the appearance of a number of chemostratigraphic anomalies in the Nhi Tao section, all of which persist into the Lower Triassic to varying degrees. There is an abrupt and sustained decline in organic matter (OM) burial, as reflected in TOC concentrations (Fig. 5), which may be evidence of a near-total collapse of contemporaneous marine primary productivity at a local or larger scale (cf. Grice et al., 2005). This is remarkable in view of the paleogeographic location of the Nhi Tao section along the southern margin of the South China Craton (Fig. 2), where nutrient-rich ocean currents would have been likely to sustain productivity under normal conditions. Such a productivity crash may indicate the end-Permian demise not only of the contemporaneous marine macrofauna but also of microscopic primary producers (Rhodes and Thayer, 1991; Erwin et al., 2002; Isozaki et al., 2007-this volume). Such a complete collapse of the Late Permian marine ecosystem may have occurred through a general poisoning of the environment, e.g., as a result of influx of anoxic (sulfidic) waters onto the Jinxi Platform. The inference that low TOC values are inconsistent with anoxia because a lack of dissolved oxygen generally enhances OM preservation (e.g., Krull et al., 2004, p. 311) overlooks that (1) OM export from surface waters will be low following a productivity crash, regardless of ambient redox conditions, and (2) even brief episodes of anoxia, if sufficiently intense, may have been sufficient to kill off the Late Permian macrobiota, and newly “sterilized” shallow-marine environments may have rapidly returned to oxic conditions (see Section 5.6 for discussion of delayed Early Triassic biotic recovery).

S concentration data provide some of the most diagnostic evidence for the character of the environmental disturbances that affected the Nhi Tao area in the latest Permian. The eight peaks in total and pyrite [S] (S1 to S8) at and above the LPEH are anomalous because an almost complete lack of sedimentary organic matter was available to drive porewater sulfate reduction in this part of the section (Fig. 5). Petrographic observations of the equivalent horizon at Dawen, China (see Section 4.1) demonstrate the occurrence of pyrite as uniformly small framboids, suggesting a syngenetic origin (i.e., precipitation from an H_2S-bearing water column; cf. Nielsen and Shen, 2004; Wignall et al., 2005). In view of the absence of sedimentologic or geochemical evidence for restricted or stagnant environmental conditions at Nhi Tao, the occurrence of syngenetic pyrite would be unusual and imply that the H_2S was not sourced within the Nhi Tao environment but, rather, imported in large quantities.

5.2. Carbonate $\delta^{13}C$ event stratigraphy

The negative shift in carbonate $\delta^{13}C$ values across the PTB at Nhi Tao (Fig. 5) is similar to, although perhaps better resolved than, similar shifts in many other PTB records (Baud et al., 1989; Holser et al., 1991; Baud et al., 1996; Jin et al., 2000; Twitchett et al., 2001; Sephton et al., 2002; Krystyn et al., 2003; Krull et al., 2004; Payne et al., 2004; Hansen, 2006). Because this shift is found at many locales worldwide, in both marine and terrestrial environments, and in both organic C and carbonate δ^{13}C records, it is unambiguously a global signal. Negative δ^{13}C shifts associated with event and/or mass extinction horizons have been attributed to (1) biomass destruction (Erwin, 1994); (2) decreased primary productivity in surface waters and reduced export of OM to deep waters (e.g., "Strangelove oceans," Hsü and McKenzie, 1985; Kump, 1991); (3) changes in the fraction of sedimentary carbon buried as organic carbon (Broecker and Peacock, 1999; Payne et al., 2004); (4) release and oxidation of methane from seafloor clathrates or bogs (Krull et al., 2000; de Wit et al., 2002); (5) upwelling of deep-ocean waters (Wignall and Twitchett, 1996; Isozaki, 1997); (6) oceanic eruption (Ryskin, 2003); (7) erosion of organic matter from continental-shelf sediments following eustatic regression (Holser and Magaritz, 1987; Faure et al., 1995; Retallack et al., 1996) or from soils following terrestrial deforestation (Looy et al., 1999; Sephton et al., 2005); and (8) volcanic CO_2 emissions (Campbell et al., 1992; Renne et al., 1995; Hansen, 2006) (see reviews in Berner, 2002; Corsetti et al., 2005). Berner (2002) concluded that no single source of ^{13}C-depleted carbon was likely to account for the variable −3 to −8‰ shifts found in PTB sections globally and that multiple factors are likely to have operated in tandem.

Patterns of geochemical covariation evident at Nhi Tao but not generally reported from other PTB sections place significant constraints on the range of viable interpretations of its C-isotopic record. Most important in this regard is the strong negative covariation exhibited by the carbonate δ^{13}C and pyrite [S] records: of eight sulfide peaks (S1 to S8), all but S4 correlate with the onset of a negative excursion in the carbonate δ^{13}C record (or with an increase in the slope of an ongoing negative excursion, as for S2; Fig. 5). From this pattern, it can be inferred that (1) multiple chemical perturbations of similar character (but somewhat variable intensity) influenced the Nhi Tao environment; and (2) reduced S and ^{12}C-enriched DIC (dissolved inorganic carbon) were introduced simultaneously during each of these events. The first perturbation, in conjunction with the LPEH, was probably the most intense, as suggested by the magnitudes of the associated geochemical excursions and by the concurrent demise of the Late Permian marine fauna and inferred collapse of marine primary productivity (Figs. 3, 5; cf. Kakuwa and Matsumoto, 2006). Subsequent events were of lesser intensity, especially those above peak S6. The fact that the sulfide peaks in the Nhi Tao section are found within narrower stratigraphic intervals (<20 cm) than the associated C-isotope excursions (~30–100 cm) reflects differences in the residence time of DIC in the modern oceanic mixed layer (~10 to 15 kyr; Berner and Berner, 1987) is substantially longer than that for H_2S in permanently euxinic water bodies such as the Black Sea (~250 yr; Lein and Ivanov, 1991).

5.3. Diagenetic control of chemostratigraphic patterns?

It is necessary to consider the scale (local versus regional or global) and timing (primary versus diagenetic) of controls on chemostratigraphic patterns observed in the Nhi Tao section. Although the −3‰ shift in the carbonate δ^{13}C record above the LPEH (Fig. 5) is indisputably a global signal, other geochemical features might potentially represent purely local influences, possibly of secondary (diagenetic) origin. However, a number of considerations favor interpretation of essentially all of chemostratigraphic patterns of the Nhi Tao section in terms of regional environmental controls. First, the facies succession, i.e., Late Permian cherty fossiliferous wackestones–packstones yielding to *Renalcis*-type calcimicrobial framestones above the LPEH (Fig. 3), is nearly identical to that found in sections across southern China (Kershaw et al., 1999; Lehrmann et al., 2001; Kershaw et al., 2002; Lehrmann et al., 2003; Ezaki et al., 2003; Lehrmann et al., 2005, 2007-this volume) as well as at some other locales globally (Baud et al., 2005). Where analyzed, these sections have yielded TOC and carbonate δ^{13}C records similar to those at Nhi Tao (e.g., Cao et al., 2002; Korte et al., 2004; Krull et al., 2004). Similar changes in microfacies and sediment geochemistry over wide areas are evidence of a regional or global environmental control. Second, the decrease in TOC values from the intensely bioturbated sediments below the LPEH (Beds 1–7) to the largely unbioturbated microbial framestones above the LPEH (Beds 9 and higher; Fig. 5) is anomalous. Microbial mats not uncommonly preserve significant quantities of OM, in no small part due to a lack of bioirrigation of the sediment (Walsh and Lowe, 1999; Decho et al., 2005). This consideration suggests that TOC patterns at Nhi Tao (and across South China) do not reflect preservational biases but, rather, differences in the original OM content of the sediment and, hence, probably also in marine primary productivity. Third, the abrupt decline in TOC at the LPEH occurred concurrently with the onset of the −3‰ shift in carbonate δ^{13}C values that is indisputably a global signal (Fig. 5). If the TOC record were controlled by local (diagenetic) processes, then this correlation would be a remarkable coincidence. A simpler explanation is that the TOC record reflects environmental controls at a regional or larger scale.

Finally, patterns of covariation among pyrite [S], pyrite $\delta^{34}S$, and carbonate $\delta^{13}C$ strongly favor an environmental control over a diagenetic one. Although covariation between the pyrite [S] and carbonate $\delta^{13}C$ records might result from variations in the intensity of sulfate reduction within the sediment in conjunction with precipitation of variable amounts of diagenetic calcite having a ^{13}C-depleted isotopic composition, there are several problems with this scenario. First, the negative $\delta^{13}C$ excursions are not stratigraphically centered around the sulfide peaks, as might be expected for a process occurring within the sediment (e.g., Taylor and Macquaker, 2000). The fact that each C-isotope excursion commences at a sulfide peak and continues for 20 to >50 cm further upsection suggests that these records represent environmental signals controlled by differences in the residence time of DIC and H_2S in seawater (see Section 5.2). Second, it is unclear that sulfate reduction could have occurred within the sediment, given the near-total lack of preserved OM above the LPEH. Complete destruction of OM through diagenesis would be highly unusual, especially in view of the preservation of measurable quantities of OM below the LPEH (Fig. 5). Third, Rayleigh distillation within a (semi-)closed diagenetic system generally results in positive covariation between pyrite [S] and pyrite $\delta^{34}S$ because the more S-rich samples contain greater quantities of ^{34}S-enriched late-stage sulfide (Goldhaber and Kaplan, 1974; Chanton et al., 1991; Mossmann et al., 1991). In contrast, there is strong negative covariation between pyrite [S] and pyrite $\delta^{34}S$ in the Nhi Tao section (Algeo et al., in review; see Section 5.4). Collectively, these considerations suggest that diagenetic processes cannot account for the chemostratigraphic patterns observed in the Nhi Tao

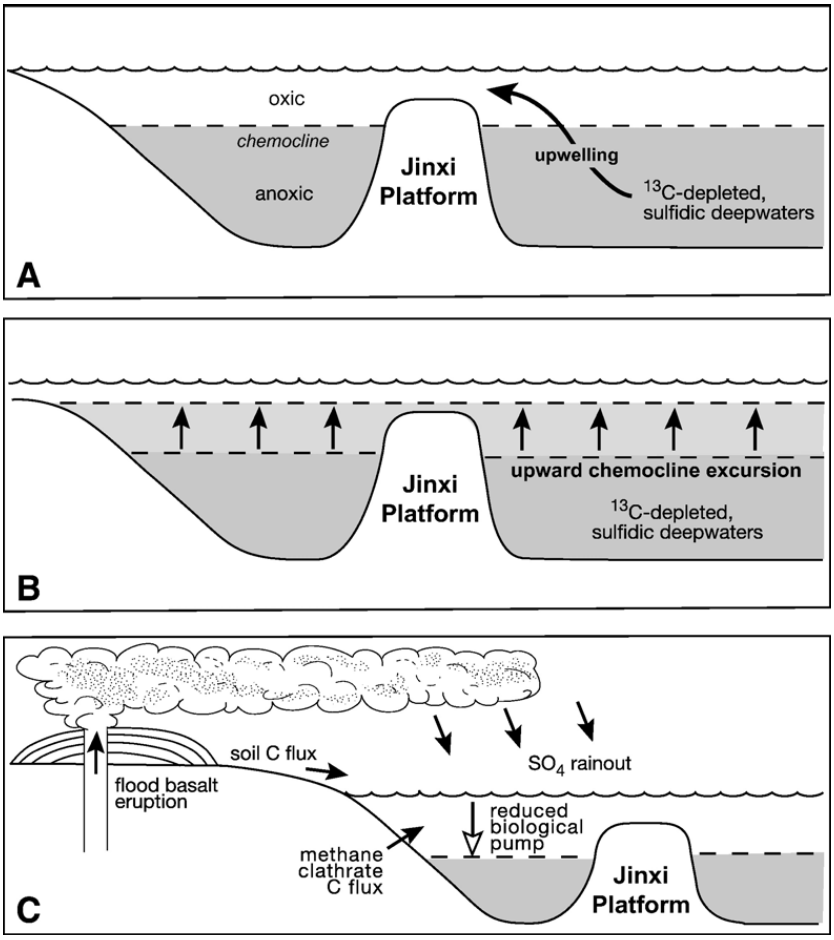

Fig. 9. Models for concurrent changes in S fluxes and carbonate $\delta^{13}C$ values. (A) Upwelling of ^{13}C-depleted, sulfide-rich deepwaters (e.g., Kajiwara et al., 1994). (B) Upward chemocline excursion, flooding shallow-marine areas with ^{13}C-depleted, sulfide-rich deepwaters (Kump et al., 2005). (C) Volcanism results in S deposition through rainout of sulfate aerosols; surface-water DIC becomes ^{13}C-depleted through deforestation and erosion of soil organic carbon (Sephton et al., 2005), oxidation of destabilized methane clathrates (Krull et al., 2000), and/or reduced surface-water productivity (Kump, 1991; Broecker and Peacock, 1999).

PTB section, and that the main environmental controls were of regional or larger scale operation.

5.4. Environmental models for PTB events at Nhi Tao

Evidence discussed above suggests that mixing of watermasses of dissimilar chemistry may have occurred on the Jinxi carbonate platform during and following the LPEH. Perhaps the most likely scenario is episodic mixing of oxic, ^{13}C-enriched surface waters with sulfidic, ^{13}C-depleted deepwaters (Fig. 9A; cf. Malkowski et al., 1989; Hoffman et al., 1991; Gruszczynski et al., 1992). Upwelling of sulfidic deep-ocean waters as a cause of the Late Permian mass extinction of shallow-marine biota has been invoked in earlier studies based on evidence of (1) thin pyritic or ferruginous clay layers at or above the LPEH (Isozaki, 1994; Shukla et al., 2000; Yin et al., 2001; Wignall et al., 2005; Grasby and Beauchamp, in review); (2) episodes of ^{32}S enrichment of both pyrite sulfide and carbonate-associated sulfate (CAS), interrupting a long-term Late Permian–Early Triassic trend toward heavier δ^{34}S values (Wignall and Hallam, 1992; Kajiwara et al., 1994; Knoll et al., 1996; Wignall and Twitchett, 1996; Wignall et al., 1998; Kaiho et al., 2001; Newton et al., 2004; Nielsen and Shen, 2004; Grice et al., 2005; Marenco et al., 2005); and (3) Ce anomalies (Kato et al., 2002; Kakuwa and Matsumoto, 2006). Covariation of carbonate δ^{13}C and pyrite [S] similar to that documented in the present study (Fig. 5) appears to be unreported to date, although such patterns may be manifested in a few published Permian–Triassic datasets (e.g., Garntnerkofel, Austria, Holser et al., 1991, their figure 10; and Festningen, Spitsbergen, Wignall et al., 1998, their Fig. 4 and Paul Wignall, pers. comm., 2006).

A second hypothesis to account for chemostratigraphic patterns at Nhi Tao is upward chemocline excursion (Fig. 9B; Kump et al., 2005). During such excursions, the O_2–H_2S redox boundary rises toward the ocean surface and, in some cases, H_2S is released to the atmosphere. A massive, short-term influx of deep-ocean H_2S in to the ocean surface and atmosphere might have had catastrophic consequences while leaving only a subtle sedimentary signal owing to rapid oxidation of the released H_2S. One factor that may have contributed to upward chemocline excursion is low atmospheric O_2 levels, which have been inferred for the PTB interval on the basis of geochemical, paleontologic, and modeling studies (Hoffman et al., 1990; Sheldon and Retallack, 2002; Retallack et al., 2003; Weidlich et al., 2003; Berner, 2005; Huey and Ward, 2005). Either mechanism (upwelling or upward chemocline excursion) could account for the Late Permian mass extinction, as relatively modest concentrations of H_2S are toxic to both marine and terrestrial life (Bagarinao, 1992). However, it is unclear whether the depth of the oceanic chemocline could have fluctuated much at the short timescales (~20 kyr) associated with recurrent episodes of sulfide influx into the Nhi Tao environment. Alternatively, it is possible that stagnation of the global ocean led to a general upward chemocline excursion during the Late Permian, and that this development facilitated the introduction of sulfidic waters to shallow-marine environments through episodic short-term upwelling events triggered by other factors.

A third hypothesis is deposition of sulfur directly from aerosols following a series of volcanic eruptions (Fig. 9C). Although such a model might be able to account for covariation of pyrite [S] and carbonate δ^{13}C values if each eruptive event triggered renewed deepwater upwelling (e.g., through volcanically induced climate cooling), S-isotopic data make a volcanic source for the sulfide peaks (S1–S8) at Nhi Tao highly unlikely. A subset of Nhi Tao samples was analyzed for pyrite δ^{34}S, which ranged from −37.9 to +7.0‰ with 15 of 25 values <−20‰ (Algeo et al., in review). The majority of these values are inconsistent with volcanic S emissions, which generally yield sulfide and sulfate δ^{34}S values within a few per mille of the mantle value of 0‰ (Ripley et al., 2003), although the S-isotopic composition of magmas can vary somewhat as a function of oxygen fugacity (Sakai et al., 1982, 1984). On the other hand, pyrite δ^{34}S values of −40 to −20‰, which are common in other marine PTB sections also (e.g., Kajiwara et al., 1994; Nielsen and Shen, 2004), are consistent with a deepwater source in which H_2S was generated through dissimilatory sulfate reduction in an open (non-S-limited) system (Goldhaber and Kaplan, 1974; Habicht and Canfield, 2001). Given a Late Permian seawater sulfate δ^{34}S of ~+10‰ (Strauss, 1997), these values represent fractionations of ~−30 to −50‰ relative to the source. Algeo et al. (in review) also identified a significant negative correlation between pyrite [S] and δ^{34}S values ($r = -0.68$; $p(\alpha) < 0.01$). Modeling of this relationship demonstrated its possible origin through mixing of a sulfide-poor endmember having δ^{34}S ~+5‰ (e.g., Late Permian surface-ocean waters) and a sulfide-rich endmember having δ^{34}S ~−45‰ (e.g., Late Permian deep-ocean waters). In combination with the pattern of carbonate δ^{13}C-pyrite [S] documented above, these observations appear to refute direct volcanic control of chemostratigraphic variation at Nhi Tao and to favor an upwelling model.

If upwelling is accepted as the major mechanism responsible for PTB events recorded in the Nhi Tao section, then certain other, previously enigmatic chemostratigraphic patterns can be explained. First, the carbonate $\delta^{13}C$ record exhibits quasi-cyclic fluctuations of 0.5 to 1.0‰ at intervals of 50 to 150 cm throughout the Lower Triassic part of the section (Fig. 5). These "meter-scale" cycles can be attributed to episodes of upwelling of ^{13}C-depleted deepwaters at quasi-regular intervals, with more (less) ^{13}C-depleted values associated with intensified (reduced) upwelling. The fact that there is some recovery of surface waters toward more ^{13}C-enriched values between each upwelling episode indicates that the "biological pump" was still operating and that the productivity of Early Triassic surface waters had not been reduced to zero. A simple calculation based on the "Strangelove ocean" model of Kump (1991) suggests that the Nhi Tao environment experienced a sustained decrease in marine primary productivity of ~50% following the LPEH, i.e., $(+2‰ - (-1‰))/(+2‰-(-5‰))$, where +2‰ is the pre-LPEH baseline for $\delta^{13}C_{carb}$, −1‰ the post-LPEH quasi-equilibrium value, and −5‰ the long-term equilibrium value for a sterile ocean. This estimate is consistent both with the inference of reduced primary productivity based on TOC data as well as with evidence of continued operation of the "biological pump" provided by fluctuations in carbonate $\delta^{13}C$ (Fig. 5). Based on sedimentation rate estimates for Nhi Tao (see Section 4.2), the ~6 m of section above the PTB represents ~100 kyr and, hence, the five "meter-scale" cycles represent ~20 kyr each. This timescale may indicate control of upwelling rates through changes in climate or atmospheric circulation driven by Earth's ~20-kyr orbital precession cycle. Thus, the Nhi Tao section appears to offer a high-resolution window into earliest Triassic environmental and paleoceanographic dynamics.

A second enigmatic feature that may be explained by an upwelling model is the P1 phosphorus anomaly. Whereas the P2 and P3 anomalies are clearly associated with the high-detrital intervals D2 and D3 (Fig. 4) and, hence, probably owe their genesis to enhanced retention of reactive P within the sediment as a function of greater concentrations of ferric Fe (Jarvis et al., 1994; McManus et al., 1997), the P1 anomaly clearly predates the D1 detrital interval (Fig. 5). The most significant aspect of the P1 anomaly is its stratigraphic position within the highly sulfidic interval bracketed by peaks S1 and S6 (but at a gap between sulfide peaks) and at the *termination* of the rapid −3‰ decrease in carbonate $\delta^{13}C$ values across the PTB (Fig. 5). A possible origin for this anomaly that is consistent with other observations and inferences pertaining to the Nhi Tao section is: (1) buildup of large quantities of reactive P in the anoxic deep-ocean watermass as sinking organic matter was remineralized and not retained by the sediment (e.g., Ingall et al., 1993); (2) introduction of large quantities of reactive P to surface waters in conjunction with the deepwater upwelling events that produced sulfide peaks S1–S6; and (3) transfer of this P to the sediment in the Nhi Tao environment during a brief interval between the S2 and S3 sulfide peaks when watermass conditions became sufficiently oxidizing to convert ferrous Fe to ferric Fe and allow P retention (e.g., Jarvis et al., 1994). Thus, the P1 peak may reflect chemical paleoceanographic dynamics at Nhi Tao rather than the influence of bulk lithology on early diagenetic redox processes, as is likely for the P2 and P3 anomalies.

5.5. MS event stratigraphy and terrestrial influence

The Nhi Tao magnetic susceptibility (MS) record may provide important additional insights regarding processes affecting the Jinxi Platform during the PTB interval. All mineral grains are susceptible to magnetization in the presence of a magnetic field, and MS measures the strength of such transient magnetism in a sample. In applied low-strength inducing magnetic fields, MS is largely a function of the concentration and grain morphology of more strongly magnetizable mineral phases (Ellwood et al., 2000). However, it is also a directional property that depends on the distribution of mineral grains and on the MS anisotropy of individual grains. In sediments, magnetizable phases include not only the ferrimagnetic and antiferromagnetic minerals (e.g., Fe-oxide minerals such as magnetite and maghemite, and Fe-sulfide minerals such as pyrrhotite and greigite) that may acquire remanent magnetization, but also other less strongly magnetic ("paramagnetic") phases. The latter group includes clay minerals (e.g., chlorite, smectite, and illite), ferromagnesian silicates (e.g., biotite, pyroxene, and amphiboles), Fe-sulfides (e.g., pyrite and marcasite), Fe-carbonates (e.g., siderite and ankerite), and other iron- and magnesium-bearing minerals. Other sedimentary phases, including calcite, quartz, and organic matter, typically acquire a weak negative MS when placed in an inducing magnetic field. Because the MS signal of such "diamagnetic" phases is opposite that of the applied field, their presence reduces total sample MS.

An important feature of the Nhi Tao MS record is the abrupt latest Permian shift from the very low values characteristic of samples containing high concentrations of diamagnetic calcite (Beds 1–8) to the much higher values where the MS signal is dominated by paramagnetic minerals, here primarily illite (Beds 9 and higher; Figs. 7 and 8). The source of the increased flux of these mineral phases at Nhi Tao (and in other PTB sections, e.g., Hansen et al., 2000) is probably fine detrital siliciclastics produced through enhanced subaerial erosion. Such erosive events have been linked to eustatic falls or climate/weathering rate changes (e.g., Ellwood et al., 1999, 2000, 2001; Crick et al., 2002; Hassold et al., 2003; Kissel et al., 2003), but for the PTB a more likely possibility is disturbance of terrestrial ecosystems and subsequent soil mobilization (Sephton et al., 2005). Evidence for this process includes (1) polysaccharide-rich, soil-derived organic matter in marine deposits (Sephton et al., 2001; Visscher et al., 2004; Sephton et al., 2005; Watson et al., 2005; Wang and Visscher, 2007-this volume); (2) pedoliths (redeposited soils) (Retallack, 2005); (3) a shift from meandering to braided stream systems (Newell et al., 1999; Ward et al., 2000; Michaelsen, 2002); and (4) a widespread expansion of herbaceous plants at the expense of woody vegetation (Retallack et al., 1996; Looy et al., 1999, 2001). Unlike some other PTB sections, the Nhi Tao section was sufficiently isolated on the distal margin of the Nanpanjiang Basin that it received only limited quantities of fine detrital material through this process, limiting the change in its bulk lithology through the PTB interval (n.b., continued accumulation of limestone despite the demise of most metazoan carbonate secreters reflects the near-saturated condition of tropical ocean-surface waters with respect to calcium carbonate, which must be precipitated either biotically or abiotically in order to maintain the chemical equilibrium of seawater).

The high resolution afforded by the Nhi Tao section allows the relative sequence of penecontemporaneous events in the marine and terrestrial environments to be assessed. The major Late Permian MS shift (base of MS1; Fig. 4) does not correlate with the LPEH at the base of Bed 8 but, rather, is found 12 cm higher at the base of Bed 9 (Fig. 3). If the LPEH and the MS shift were causally related, as seems likely, then the latter event was recorded in the Nhi Tao marine environment with a distinct time lag. Further, lags are also associated with the MS2 and MS3 horizons, which follow sulfide peaks S7 and S8 at intervals of ~10 and 50 cm, respectively (Figs. 4 and 5). These lags probably represent the time required for mobilization and transport of (soil-derived?) clays across the Nanpanjiang Basin to the distal Jinxi Platform. Based on a section-average sedimentation rate of 15 mm kyr^{-1}, these lags are equivalent to ~7 to 30 kyr; however, the 12-cm-thick oolitic–pisolitic grainstone of Bed 8 (representing the MS1 lag) might have been deposited much faster, in a matter of years(?) to centuries(?), if abiotic grain precipitation was a response to a perturbation that caused strong carbonate supersaturation of surface waters in the Nhi Tao environment. On the other hand, the onset of each high-MS horizon (MS1 to MS3) precedes an increase in detrital-fraction abundance (horizons D1 to D3) by an interval of ~20 to 50 cm (Fig. 4). MS records commonly exhibit a close relationship to detrital grain size (e.g., Ellwood et al., 2000; Hassold et al., 2003; Kissel et al., 2003), so this pattern may reflect more rapid (eolian?) transport of the fine detrital components carrying the bulk of the MS signal relative to the slower-moving illite fraction. These stratigraphic relationships demonstrate that, during each perturbation of the Nhi Tao environment, the chemical oceanographic signal was recorded in advance of the terrestrial signal. Owing to the probable time lag associated with the latter, however, the most parsimonious interpretation may be that regional changes in marine and terrestrial changes were synchronous responses to large-scale oceanic–atmospheric perturbations.

5.6. Speculations concerning global significance

The evidence discussed above for multiple episodes of upwelling of sulfidic deep-ocean waters and for possibly synchronous perturbations of marine and terrestrial systems imposes significant constraints on models for the latest Permian catastrophe and mass extinction. Although the present study is limited to a single locale, the widespread evidence for upwelling of sulfidic deepwaters at the PTB (Kajiwara et al., 1994; Knoll et al., 1996; Wignall and Twitchett, 1996; Wignall et al., 1998; Kaiho et al., 2001; Kato et al., 2002; Newton et al., 2004; Nielsen and Shen, 2004; Grice et al., 2005; Marenco et al., 2005) suggests a global-scale process. This may imply that such upwelling events represent transient reinvigoration of global-ocean overturn following a protracted interval of near-stagnant conditions during the Late Permian, during which the deep ocean became widely anoxic and sulfidic (Malkowski et al., 1989; Hoffman et al., 1991; Gruszczynski et al., 1992; Wignall and Hallam, 1992; Isozaki, 1994; Kajiwara et al., 1994; Isozaki, 1997; Hotinski et al., 2001). A plausible mechanism to account for the abrupt initiation of upwelling at the LPEH is the approximately simultaneous onset of eruption of the Siberian Traps (Campbell et al., 1992; Renne et al., 1995; Kamo et al., 2003). However, volcanic processes are unlikely to have induced subsequent episodes of upwelling at quasi-regular intervals of ~20 kyr (e.g., Lin and van Keken, 2005), as recorded in the Nhi Tao PTB section. Rather, a more likely scenario is that a single massive volcanic eruption at ~251 Ma caused strong climatic cooling, bringing the global ocean closer to a threshold for renewed overturn, and that precession-driven climate cycles modulated subsequent upwelling episodes.

This model has some significant implications with regard to the extinction and recovery of Permian–Triassic marine life. First, although the ultimate trigger for PTB events may have been volcanic, the demise of the Late Permian marine biota may have been due to largely internal oceanographic factors, i.e., upwelling of toxic deepwaters (although climatic cooling might have been a factor as well). Multiple upwelling events may account for reports of multiple extinction horizons in Chinese PTB sections (e.g., Jin et al., 2000; Xie et al., 2005). Second, recurrent upwelling of toxic deep-ocean waters may have been an important factor in delaying the post-extinction recovery of marine ecosystems, which did not rebound substantially until the early Middle Triassic, approximately 6 Myr after the PTB event (Schubert and Bottjer, 1992, 1995; Knoll et al., 1996; Baud et al., 1997; Sano and Nakashima, 1997; Kershaw et al., 1999; Lehrmann, 1999; Twitchett, 1999; Kershaw et al., 2002; Twitchett, 2005; Ezaki et al., 2003; Lehrmann et al., 2001, 2003; Weidlich et al., 2003; Fraiser and Bottjer, 2004; Pruss and Bottjer, 2004; Payne, 2005; Payne et al., 2006). Although originally attributed to poor Lower Triassic fossil preservation or to the time needed for reintegration of marine ecosystems (Erwin, 1994; Erwin et al., 2002), this delay has more recently been interpreted to reflect persistently inhospitable conditions in Early Triassic marine environments (Hallam, 1991; Wignall and Twitchett, 2002; Twitchett et al., 2004). Continued perturbation of Early Triassic environments is suggested by evidence of multiple, large fluctuations in marine carbonate δ^{13}C records through the Lower Triassic (Payne et al., 2004; Korte et al., 2005; Horacek et al., 2007-this volume-a-b). The multiple δ^{13}C excursions documented in this study (Fig. 5), although smaller in amplitude and shorter in duration than these million-year-long Early Triassic cycles (Fig. 1), are nonetheless significant in demonstrating that quasi-cyclic carbon-cycle perturbations were operating at a high (~20-kyr) frequency following the LPEH (cf. de Wit et al., 2002). The deepwater upwelling model discussed herein may provide a mechanism for the protracted Early Triassic marine crisis, although other factors must be invoked to account for coeval disturbance of terrestrial ecosystems (Retallack et al., 1996; Korte et al., 2003, 2005).

Several recent studies have argued that the PTB negative C-isotopic shift post-dates the end-Permian mass extinction and, thus, represents a delayed response to the catastrophe, e.g., associated with release of methane clathrates owing to volcanically induced climate warming (Twitchett et al., 2001; Krull et al., 2004; Sephton et al., 2005). However, the onset of the negative δ^{13}C shift at Nhi Tao is found in the lower part of the LPEH event bed (Bed 8), in the first sample above the mass extinction horizon, with which it was thus synchronous within the limits of sampling resolution (Fig. 3). Further, the *onset* of the negative δ^{13}C shift appears to be correlative with the mass extinction horizon in other PTB sections (e.g., Krull et al., 2004, their Figs. 6 and 7). Inferences to the contrary seem to reflect a misperception that the *minimum* of the C-isotopic shift should correlate with the mass extinction horizon (e.g., Krull et al., 2004, their Fig. 8). In fact, the relatively long residence time of DIC in the oceanic mixed layer (~10 to 15 kyr; Berner and Berner, 1987) limits the rate at which its isotopic composition can adjust to external perturbations, resulting in displacement of the δ^{13}C minimum upsection relative to the event horizon recording the perturbation. In simple geochemical reservoir models, the response time of the system is similar to the residence time of the compound of interest (Rodhe, 1992), so the δ^{13}C minimum in PTB C-isotope records should follow the perturbation that initiated the excursion with a lag approximately equal to the residence time of DIC in seawater. It is possible, of course, that PTB C-isotopic curves record responses to multiple influences (e.g., Berner, 2002), some instantaneous (or nearly so) and some with discrete lags.

The results of the present study also raise several issues concerning a recent model invoking deforestation and massive soil erosion following large-scale volcanic eruptions as the cause of the latest Permian marine crisis (Sephton et al., 2005). Support cited for this model includes (1) fossil evidence of changes in terrestrial ecosystems prior to the marine biotic crisis (Looy et al., 2001; Twitchett et al., 2001), and (2) molecular evidence of the influx of soil-derived compounds to marine environments prior to the LPEH (Sephton et al., 2002, 2005; Wang and Visscher, 2007-this volume). The fossil evidence for the timing of ecosystem changes is difficult to evaluate, and the possibility of an unrecognized Signor–Lipps effect must be considered (Rampino and Adler, 1998). The molecular evidence is intriguing, yet it is unclear why the signal of soil-derived compounds appears in the marine record considerably in advance of the MS signal associated with the influx of fine detrital (presumably soil-derived) particles, which post-dates the LPEH at Nhi Tao and Meishan D (Figs. 3, 7). Although terrestrial-marine coupling undoubtedly occurred, there may be other evidence to support largely separate mechanisms for the terrestrial and marine crises in the latest Permian (even if both had the same volcanic trigger). For example, sulfide enrichments in terrestrial PTB sections exhibit δ^{34}S values of −12 to +3‰ (Maruoka et al., 2003), which are similar to values reported for Siberian flood basalts (Ripley et al., 2003) but much higher than penecontemporaneous marine sulfides (see Section 5.4). This may imply two distinct sulfide sources, i.e., a largely volcanic one for terrestrial PTB sections and a largely oceanic one (via upwelling) for marine PTB sections. These issues will require further investigation to resolve.

6. Conclusions

The PTB section at Nhi Tao, Vietnam is lithologically homogeneous, facilitating recognition of changes in the hydrogenous (i.e., seawater-derived) fraction of the sediment that may represent contemporaneous changes in paleocean chemistry. The Late Permian event horizon (LPEH) at which most Late Permian faunal elements disappear coincides with a 12-cm-thick oolitic–pisolitic grainstone layer that also marks the appearance of several geochemical anomalies that continue into the Lower Triassic part of the section. Eight pyrite [S] peaks within a 5-m-thick interval above the LPEH exhibit a strong negative relationship to both carbonate δ^{13}C and pyrite δ^{34}S (i.e., higher S concentrations associated with isotopically more depleted values). The most likely mechanism to account for these relationships is episodic upwelling of sulfidic, ^{12}C- and ^{32}S-enriched deep-ocean waters onto the shallow Jinxi Platform. Such quasi-cyclic episodes of upwelling may represent multiple attempts at renewed global-ocean overturn modulated by Earth's 20-kyr orbital precession cycle following prolonged stagnation of the deep ocean during the Late Permian. Large-scale upwelling of deepwaters implies that the end-Permian marine mass extinction was caused by anoxia and/or sulfide toxicity, and that recurrent episodes during the Early Triassic may have been a factor in delaying significant recovery of marine ecosystems until the start of the Middle Triassic. The rate and magnitude (−3‰) of the carbonate δ^{13}C shift across the PTB at Nhi Tao are consistent with a "Strangelove ocean" model with a sustained ~50% decline in primary productivity. A major increase in MS values 12 cm above the LPEH may record an influx of fine soil-derived particles following destruction of terrestrial ecosystems. The lag is consistent with the interval required for transport of fine particles across the Nanpanjiang Basin to the relatively distal site of the Jinxi Platform. Within existing limits of uncertainty, the end-Permian marine and terrestrial crises recorded at Nhi Tao appear to have occurred synchronously.

Acknowledgments

We thank Deirdre McCartney, Jon Wetterich, and Warren Huff (U. Cincinnati) and Bob King (U. Kentucky) for laboratory assistance, Hans Jørgen Hansen for Meishan D magnetic susceptibility data, and Lee Kump, Richard Twitchett, and an anonymous reviewer for constructive reviews of the manuscript. This project was supported by grants to TJA from the National Science Foundation (EAR-0310072 and EAR-0618003) and the University of Cincinnati Research Council.

References

Algeo, T.J., Maynard, J.B., 2004. Trace element behavior and redox facies in core shales of Upper Pennsylvanian Kansas-type cyclothems. Chem. Geol. 206, 289–318.

Algeo, T.J., Hannigan, R., Rowe, H., Brookfield, M., Baud, A., Krystyn, L., Ellwood, B.B., 2007. Sequencing events across the Permian-Triassic boundary, Guryul Ravine (Kashmir, India). Paleogeogr. Paleoclimatol. Paleoecol. 252, 328–346 (this volume). doi:10.1016/j.palaeo.2006.11.050.

Algeo, T.J., Shen, Y., Zhang, T., Lyons, T.W., Bates, S.M., Rowe, H., Nguyen, T.K.T., in review. Renewed deep-ocean overturn and the Permian-Triassic boundary mass extinction. Geology, submitted March, 2007.

Arp, G., Reimer, A., Reitner, J., 2003. Microbialite formation in seawater of increased alkalinity, Satonda Crater Lake, Indonesia. J. Sediment. Res. 73, 105–127.

Bachmann, G.H., Kozur, H.W., 2004. The Germanic Triassic: correlations with the international chronostratigraphic scale, numerical ages and Milankovitch cyclicity. Hallesches Jahrb. Geowiss., B Geol. Palaontol. Mineral. 26, 17–62.

Bagarinao, T., 1992. Sulfide as an environmental factor and toxicant: tolerance and adaptations in aquatic organisms. Aquat. Toxicol. 24, 21–62.

Basu, A.R., Petaev, M.I., Poreda, R.J., Jacobsen, S.B., Becker, L., 2003. Chondritic meteorite fragments associated with the Permian–Triassic boundary in Antarctica. Science 302, 1388–1392.

Basu, A.R., Poreda, R.J., Renne, P.R., Sobolev, N.V., Teichmann, F., Turrin, B.D., Vasiliev, Y.R., 1995. High-^{3}He plume origin and temporal–spatial evolution of the Siberian flood basalts. Science 269, 822–825.

Baud, A., Holser, W.T., Magaritz, M., 1989. Permian–Triassic of the Tethys; Carbon isotope studies. Geol. Rundsch. 78, 649–677.

Baud, A., Atudorei, V., Sharp, Z., 1996. Late Permian and Early Triassic evolution of the Northern Indian margin: carbon isotope and sequence stratigraphy. Geodyn. Acta (Paris) 9, 57–77.

Baud, A., Cirilli, S., Marcoux, J., 1997. Biotic response to mass extinction: the lowermost Triassic microbialites. Facies 36, 238–242.

Baud, A., Richoz, S., Marcoux, J., 2005. Calcimicrobial cap rocks from the basal Triassic units: western Taurus occurrences (SW Turkey). C.R. Palevol, 4, pp. 501–514.

Becker, L., Poreda, R.J., Hunt, A.G., Bunch, T.E., Rampino, M., 2001. Impact event at the Permian–Triassic boundary: evidence from extraterrestrial noble gases in fullerenes. Science 291, 1530–1533.

Becker, L., Poreda, R.J., Basu, A.R., Pope, K.O., Harrison, T.M., Nicholson, C., Iasky, R., 2004. Bedout: a possible end-Permian impact crater offshore of northwestern Australia. Science 304, 1469–1476.

Benton, M.J., 2003. When Life Nearly Died: The Greatest Mass Extinction of all Time. Thames and Hudson, London. 336 pp.

Benton, M.J., Twitchett, R.J., 2003. How to kill (almost) all life: the end-Permian extinction event. Trends Ecol. Evol. 18, 358–365.

Berner, R.A., 2002. Examination of hypotheses for the Permo-Triassic boundary extinction by carbon cycle modeling. Proc. Natl. Acad. Sci. 99, 4172–4177.

Berner, R.A., 2005. The carbon and sulfur cycles and atmospheric oxygen from middle Permian to Middle Triassic. Geochim. Cosmochim. Acta 69, 3211–3217.

Berner, E.K., Berner, R.A., 1987. The Global Water Cycle. Prentice-Hall, Englewood Cliffs, New Jersey. 397 pp.

Bowring, S.A., Erwin, D.H., Jin, Y.G., Martin, M.W., Davidek, K., Wang, W., 1998. U/Pb zircon geochronology and tempo of the end-Permian mass extinction. Science 280, 1039–1045.

Bowring, S.A., Erwin, D.H., Isozaki, Y., 1999. The tempo of mass extinction and recovery: the end-Permian example. Proc. Natl. Acad. Sci. 96, 8827–8828.

Broecker, W.S., Peacock, S., 1999. An ecologic explanation for the Permo-Triassic carbon and sulfur isotope shifts. Glob. Biogeochem. Cycles 13, 1167–1172.

Brookfield, M.E., Twitchett, R.J., Goodings, C., 2003. Palaeoenvironments of the Permian–Triassic transition sections in Kashmir India. Palaeogeogr. Palaeoclimatol. Palaeoecol. 198, 353–371.

Campbell, I.H., Czamanske, G.K., Fedorenko, V.A., Hill, R.I., Stepanov, V., 1992. Synchronism of the Siberian Traps and the Permian–Triassic boundary. Science 258, 1760–1763.

Cao, C., Wang, W., Jin, Y., 2002. Carbon isotope excursions across the Permian–Triassic boundary in the Meishan section, Zhejiang Province, China. Chin. Sci. Bull. 47, 1125–1129.

Chanton, J.P., Martens, C.S., Paull, C.K., 1991. Control of pore-water chemistry at the base of the Florida escarpment by processes within the platform. Nature 349, 229–231.

Chen, J.-S., Chu, X.-L., Shao, M.-R., Zhong, H., 1991. Carbon isotope study of the Permian–Triassic boundary sequences in China. Chem. Geol. 89, 239–251.

Corsetti, F.A., Baud, A., Marenco, P.J., Richoz, S., 2005. Summary of Early Triassic carbon isotope records. C. R. Palevol, vol. 4, pp. 473–486.

Crick, R.E., Dreesen, R., El Hassani, A., Ellwood, B.B., Feist, R., Girard, C., Over, D.J., Schindler, E., 2002. Magnetostratigraphy susceptibility of the Frasnian/Famennian boundary. Palaeogeogr. Palaeoclimatol. Palaeoecol. 181, 67–90.

Decho, A.W., Visscher, P.T., Reid, R.P., 2005. Production and cycling of natural microbial exopolymers (EPS) within a marine stromatolite. Palaeogeogr. Palaeoclimatol. Palaeoecol. 219, 71–86.

de Wit, M.J., Ghosh, J.G., de Villiers, S., Rakotosolofo, N., Alexander, J., Tripathi, A., Looy, C., 2002. Multiple organic carbon isotope reversals across the Permo-Triassic boundary of terrestrial Gondwana sequences: clues to extinction patterns and delayed ecosystem recovery. J. Geol. 110, 227–240.

Doan, N.T., Dang, T.H., Nguyen, X.K., Ta, H.P., 2004. On the Permian/Triassic boundary in Vietnam. J. Geol. (Hanoi, Vietnam), Ser. B (24), 1–9.

Ellwood, B.B., Crick, R.E., El Hassani, A., 1999. The magnetosusceptibility event and cyclostratigraphy (MSEC) method used in geological correlation of Devonian rocks from anti-Atlas Morocco. Am. Assoc. Pet. Geol. Bull. 83, 1119–1134.

Ellwood, B.B., Crick, R.E., El Hassani, A., Benoist, S.L., Young, R.H., 2000. Magnetosusceptibility event and cyclostratigraphy method applied to marine rocks: detrital input versus carbonate productivity. Geology 28, 1135–1138.

Ellwood, B.B., Crick, R.E., Garcia-Alcalde Fernandez, J.-L., Soto, F.M., Truyóls-Massoni, M., El Hassani, A., Kovas, E.J., 2001. Global correlation using magnetic susceptibility data from Lower Devonian rocks. Geology 29, 583–586.

Erwin, D.H., 1994. The Permo-Triassic extinction. Nature 367, 231–236.

Erwin, D.H., Bowring, S.A., Jin, Y.-G., 2002. End-Permian mass-extinctions: a review. In: Koeberl, C., MacLeod, K.G. (Eds.), Catastrophic Events and Mass Extinctions: Impacts and Beyond. Geol. Soc. Am. Spec. Paper, vol. 356, pp. 353–383.

Ezaki, Y., Liu, J., Adachi, N., 2003. Earliest Triassic microbialite micro- to megastructures in the Huaying area of Sichuan Province, South China: implications for the nature of oceanic conditions after the end-Permian extinction. Palaios 18, 388–402.

Farley, K.A., Mukhopadhyay, S., 2001. An extraterrestrial impact at the Permian–Triassic boundary? Science 293, 2343a.

Faure, K., de Wit, M.J., Willis, J.P., 1995. Late Permian global coal hiatus linked to ^{13}C-depleted CO_2 flux into the atmosphere during the final consolidation of Pangea. Geology 23, 507–510.

Fraiser, M.L., Bottjer, D.J., 2004. The non-actualistic Early Triassic gastropod fauna; a case study of the Lower Triassic Sinbad Limestone Member. Palaios 19, 259–275.

Fraiser, M.L., Bottjer, D.J., 2007. Elevated atmospheric CO_2 and the delayed biotic recovery from the end-Permian mass extinction. Palaeogeogr. Palaeoclimatol. Palaeoecol. 252, 164–175 (this volume). doi:10.1016/j.palaeo.2006.11.041.

Goldhaber, M.B., Kaplan, I.R., 1974. The sulfur cycle. In: Goldberg, E.D. (Ed.), The Sea, v. 5: Marine Chemistry. John Wiley & Sons, New York, pp. 569–655.

Gorter, J.D., 1996. Speculation on the origin of the Bedout High — a large, circular structure of pre-Mesozoic age in the Offshore Canning Basin, Western Australia. Petrol. Explor. Soc. Austr. News 1996 (4), 32–33.

Gradstein, F., Ogg, J., Smith, A., 2004. A Geologic Time Scale. Cambridge Univ. Press. 589 pp.

Grasby, S.E., Beauchamp, B., in review. C-isotopes of P-T transition in Sverdrup Basin, Arctic Canada: evidence for gradual environmental deterioration leading to End-Permian extinction. Geol. Soc. Amer. Bull.

Grice, K., Cao, C., Love, G.D., Böttcher, M.E., Twitchett, R.J., Grosjean, E., Summons, R.E., Turgeon, S.C., Dunning, W., Jin, Y., 2005. Photic zone euxinia during the Permian–Triassic superanoxic event. Science 307, 706–709.

Grim, R.E., 1968. Clay Mineralogy, 2nd ed. McGraw-Hill, New York. 596 pp.

Grotzinger, J.P., Knoll, A.H., 1995. Anomalous carbonate precipitates: is the Precambrian the key to the Permian? Palaios 10, 578–596.

Gruszczynski, M., Hoffman, A., Malkowski, K., Veizer, J., 1992. Seawater strontium isotopic perturbation at the Permian–Triassic boundary, West Spitsbergen, and its implications for the interpretation of strontium isotopic data. Geology 20, 779–782.

Habicht, K.S., Canfield, D.E., 2001. Isotope fractionation by sulfate-reducing natural populations and the isotopic composition of sulfide in marine sediments. Geology 29, 555–558.

Hallam, A., 1991. Why was there a delayed radiation after the end-Palaeozoic extinction? Hist. Biol. 5, 257–262.

Handbook of Physics and Chemistry, 85th ed. CRC Press, Boca Raton, Florida.

Hansen, H.J., 2006. Stable isotopes of carbon from basaltic rocks and their possible relation to atmospheric isotope excursions. Lithos 92, 105–116.

Hansen, H.J., Lojen, S., Toft, P., Dolenec, T., Tong, J., Michaelsen, P., Sarkar, A., 2000. Magnetic susceptibility and organic carbon isotopes of sediments across some marine and terrestrial Permo-Triassic boundaries. In: Yin, H., Dickins, J.M., Shi, G.R., Tong, J. (Eds.), Permian–Triassic Evolution of Tethys and Western Circum-Pacific. Elsevier, Amsterdam, pp. 271–289.

Hassold, N., Meyers, P.A., Rea, D.K., 2003. Grain size evidence for variations in delivery of terrigenous sediments to a middle Pleistocene interrupted sapropel from ODP Site 969, Mediterranean Ridge. Palaeogeogr. Palaeoclimatol. Palaeoecol. 190, 211–219.

Heydari, E., Hassanzadeh, J., Wade, W.J., Ghazi, A.M., 2003. Permian–Triassic boundary interval in the Abadeh section of Iran with implications for mass extinction, Part 1: Sedimentology. Palaeogeogr. Palaeoclimatol. Palaeoecol. 193, 405–423.

Hoffman, A., Gruszczynski, M., Malkowski, K., 1990. Oceanic δ^{13}C values as indicators of atmospheric oxygen depletion. Mod. Geol. 14, 211–221.

Hoffman, A., Gruszczynski, M., Malkowski, K., 1991. On the interrelationship between temporal trends in δ^{13}C, δ^{18}O, and δ^{34}S in the world ocean. J. Geol. 99, 355–370.

Holser, W.T., Magaritz, M., 1987. Events near the Permian–Triassic boundary. Mod. Geol. 11, 155–180.

Holser, W.T., Schönlaub, H.P., Boeckelmann, K., Magaritz, M., 1991. The Permian–Triassic of the Gartnerkofel-1 core (Carnic Alps, Austria): synthesis and conclusions. Abh. Geol. Bundesanst. (Vienna, Austria) 45, 213–232.

Horacek, M., Brandner, R., Abart, R., 2007a. Carbon isotope record of the P/T boundary and the Lower Triassic in the Southern Alps: evidence for rapid changes in storage of organic carbon. Palaeogeogr. Palaeoclimatol. Palaeoecol. 252, 347–354 (this volume). doi:10.1016/j.palaeo.2006.11.049.

Horacek, M., Richoz, S., Brandner, R., Krystyn, L., Spötl, C., 2007b. The δ^{13}C curve of Lower Triassic marine sediments from Iran. Palaeogeogr. Palaeoclimatol. Palaeoecol. 252, 355–369 (this volume). doi:10.1016/j.palaeo.2006.11.052.

Hotinski, R.M., Bice, K.L., Kump, L.R., Najjar, R.G., Arthur, M.A., 2001. Ocean stagnation and end-Permian anoxia. Geology 29, 7–10.

Hsü, K.J., McKenzie, J.A., 1985. A "strangelove" ocean in the earliest Tertiary. In: Sundquist, E.T., Broecker, W.S. (Eds.), Carbon Cycle and Atmospheric CO_2; Natural Variations Archean to Present. Am. Geophys. Union Geophys. Monogr., vol. 32, pp. 487–492.

Huey, R.B., Ward, P.D., 2005. Hypoxia, global warming, and terrestrial Late Permian extinctions. Science 308, 398–401.

Ingall, E.D., Bustin, R.M., Cappellen, P., 1993. Influence of water column anoxia on the burial and preservation of carbon and phosphorus in marine shales. Geochim. Cosmochim. Acta 57, 303–316.

Isozaki, Y., 1994. Superanoxia across the Permo-Triassic boundary: record in accreted deep-sea pelagic chert in Japan. In: Embry, A.F., Beauchamp, B., Glass, D.J. (Eds.), Pangea: Global Environments and Resources. Canad. Soc. Petrol. Geol. Mem., vol. 17, pp. 805–812.

Isozaki, Y., 1997. Permo-Triassic boundary superanoxia and stratified superocean; records from lost deep sea. Science 276, 235–238.

Isozaki, Y., 2001. An extraterrestrial impact at the Permian–Triassic boundary? Science 293, 2343a.

Isozaki, Y., Shimizu, N., Yao, J., Ji, Z., Matsuda, T., 2007. End-Permian extinction and volcanism-induced environmental stress: Permian–Triassic boundary interval of a lower-slope facies at Chaotian, South China. Palaeogeogr. Palaeoclimatol. Palaeoecol. 252, 218–238 (this volume). doi:10.1016/j.palaeo.2006.11.051.

Jarvis, I., Burnett, W.C., et al., 1994. Phosphorite geochemistry: State-of-the-art and environmental concerns. Eclogae Geol. Helv. 87, 643–700.

Jin, Y.G., Wang, Y., Wang, W., Shang, Q.H., Cao, C.Q., Erwin, D.H., 2000. Pattern of marine mass extinction near the Permian–Triassic boundary in South China. Science 289, 432–436.

Kaiho, K., Kajiwara, T., Nakano, T., Muira, Y., Kawahata, H., Tazaki, K., Ueshima, M., Chen, Z., Shi, G.R., 2001. End-Permian catastrophe by a bolide impact: evidence of a gigantic release of sulfur from the mantle. Geology 29, 815–818.

Kajiwara, Y., Yamakita, S., Ishida, K., Ishiga, H., Imai, A., 1994. Development of a largely anoxic stratified ocean and its temporary massive mixing at the Permian–Triassic boundary supported by the sulfur isotope record. Palaeogeogr. Palaeoclimatol. Palaeoecol. 111, 367–379.

Kakuwa, Y., Matsumoto, R., 2006. Cerium negative anomaly just before the Permian and Triassic boundary event: the upward expansion of anoxia in the water column. Palaeogeogr. Palaeoclimatol. Palaeoecol. 229, 335–344.

Kamo, S.L., Czamanske, G.K., Amelin, Y., Fedorenko, V.A., Davis, D.W., Trofimov, V.R., 2003. Rapid eruption of Siberian flood-volcanic rocks and evidence for coincidence with the Permian–Triassic boundary and mass extinction at 251 Ma. Earth Planet. Sci. Lett. 214, 75–91.

Kato, Y., Nakao, K., Isozaki, Y., 2002. Geochemistry of Late Permian to Early Triassic pelagic cherts from southwest Japan: implications for an oceanic redox change. Chem. Geol. 182, 15–34.

Kershaw, S., Zhang, Ting-shan, Lan, Guang-zhi, 1999. A microbialite carbonate crust at the Permian–Triassic boundary in South China, and its palaeoenvironmental significance. Palaeogeogr. Palaeoclimatol. Palaeoecol. 146, 1–18.

Kershaw, S., Guo, Li, Swift, A., Fan, Jiang-song, 2002. Microbialites in the Permian–Triassic boundary interval in Central China: structure, age and distribution. Facies 47, 83–90.

Kiehl, J.T., Shields, C.A., 2005. Climate simulation of the latest Permian: implications for mass extinction. Geology 33, 757–760.

Kissel, C., Clemens, S., Laj, C., Solheid, P., 2003. Magnetic signature of environmental changes in the last 1.2 Myr at ODP Site 1146, South China Sea. Mar. Geol. 201, 119–132.

Knoll, A.H., Bambach, R.K., Canfield, D.E., Grotzinger, J.P., 1996. Comparative Earth history and Late Permian mass extinction. Science 273, 452–457.

Koeberl, C., Gilmour, I., Reimold, W.U., Claeys, P., Ivanov, B., 2002. End-Permian catastrophe by bolide impact: evidence of a gigantic release of sulfur from the mantle (comment). Geology 30, 855–856.

Koeberl, C., Farley, K.A., Peucker-Ehrenbrink, B., Sephton, M.A., 2004. Geochemistry of the end-Permian extinction event in Austria and Italy: no evidence for an extraterrestrial component. Geology 32, 1053–1056.

Korte, C., Kozur, H.W., Bruckschen, P., Veizer, J., 2003. Strontium isotope evolution of Late Permian and Triassic seawater. Geochim. Cosmochim. Acta 67, 47–62.

Korte, C., Kozur, H.W., Joachimski, M.M., Strauss, H., Veizer, J., Schwark, L., 2004. Carbon, sulfur, oxygen and strontium isotope records, organic geochemistry and biostratigraphy across the Permian–Triassic boundary in Abadeh, Iran. Int. J. Earth Sci. 93, 565–581.

Korte, C., Kozur, H.W., Veizer, J., 2005. δ^{13}C and δ^{18}O values of Triassic brachiopods and carbonate rocks as proxies for coeval seawater and palaeotemperature. Palaeogeogr. Palaeoclimatol. Palaeoecol. 226, 287–306.

Kozur, H.W., 2003. Integrated ammonoid, conodont and radiolarian zonation of the Triassic and some remarks to Stage/Substage subdivision and the numeric age of the Triassic stages. Albertiana 28, 57–84.

Krull, E.S., Retallack, G.J., 2000. $\delta^{13}C_{org}$ depth profiles from paleosols across the Permian–Triassic boundary: evidence for methane release. Geol. Soc. Amer. Bull. 112, 1459–1472.

Krull, E.S., Campbell, H.J., Retallack, G.J., Lyon, G.L., 2000. $\delta^{13}C_{org}$ chemostratigraphy of the Permian–Triassic boundary in the Maitai Group, New Zealand; evidence for high-latitudinal methane release. N. Z. J. Geol. Geophys. 43, 21–32.

Krull, E.S., Lehrmann, D.J., Druke, D., Kessel, B., Yu, Y., Li, R., 2004. Stable carbon isotope stratigraphy across the Permian–Triassic boundary in shallow marine carbonate platforms, Nanpanjiang Basin, south China. Palaeogeogr. Palaeoclimatol. Palaeoecol. 204, 297–315.

Krystyn, L., Richoz, S., Baud, A., Twitchett, R.J., 2003. A unique Permian–Triassic boundary section from the Neotethyan Hawasina Basin, Central Oman Mountains. Palaeogeogr. Palaeoclimatol. Palaeoecol. 191, 329–344.

Kump, L.R., 1991. Interpreting carbon-isotope excursions; Strangelove oceans. Geology 19, 299–302.

Kump, L.R., Pavlov, A., Arthur, M.A., 2005. Massive release of hydrogen sulfide to the surface ocean and atmosphere during intervals of oceanic anoxia. Geology 33, 397–400.

Lehrmann, D.J., 1999. Early Triassic calcimicrobial mounds and biostromes of the Nanpanjiang basin, South China. Geology 27, 359–362.

Lehrmann, D.J., Yang, W., Wei, J., Yu, Y., Xiao, J., 2001. Lower Triassic peritidal cyclic limestone: an example of anachronistic carbonate facies from the Great Bank of Guizhou, Nanpanjiang Basin, Guizhou province, South China. Palaeogeogr. Palaeoclimatol. Palaeoecol. 173, 103–123.

Lehrmann, D.J., Payne, J.L., Felix, S.V., Dillett, P.M., Wang, H., Yu, Y., Wei, J., 2003. Permian–Triassic boundary sections from shallow-marine carbonate platforms of the Nanpanjiang Basin, South China: implications for oceanic conditions associated with the end-Permian extinction and its aftermath. Palaios 18, 138–152.

Lehrmann, D.J., Enos, P., Payne, J.L., Montgomery, P., Wei, J., Yu, Y., Xiao, J., Orchard, M.J., 2005. Permian and Triassic depositional history of the Yangtze platform and Great Bank of Guizhou in the Nanpanjiang Basin of Guizhou and Guangxi, South China. Albertiana 33, 147–166.

Lehrmann, D.J., Payne, J.L., Pei, D., Enos, P., Ellwood, B., Orchard, M.J., Zhang, J., Wei, J., 2007. Record of the End Permian extinction and Triassic biotic recovery in the Chongzuo–Pingguo Platform, southern Nanpanjiang Basin, Guangxi, south China. Palaeogeogr. Palaeoclimatol. Palaeoecol. 252, 200–217 (this volume). doi:10.1016/j.palaeo.2006.11.044.

Lein, A.Y., Ivanov, M.V., 1991. On the sulfur and carbon balances in the Black Sea. In: Izdar, E., Murray, J.W. (Eds.), Black Sea Oceanography. Kluwer, Dordrecht, pp. 307–318.

Lepvrier, C., Leyreloup, A., Maluski, H., Vuong, N.V., Thi, P.T., Tich, V.T., 2004. The Early Triassic Indosinian Orogeny in Vietnam (Truong Son Belt and Kontum Massif); implications for the geodynamic evolution of Indochina. Tectonophysics 393, 87–118.

Lin, S.C., van Keken, P.B., 2005. Multiple volcanic episodes of flood basalts caused by thermochemical mantle plumes. Nature 436, 250–252.

Looy, C.V., Brugman, W.A., Dilcher, D.L., Visscher, H., 1999. The delayed resurgence of equatorial forests after the Permian–Triassic ecological crisis. Proc. Natl. Acad. Sci. 96, 13,857–13,862.

Looy, C.V., Twitchett, R.J., Dilcher, D.L., van Kojnijnenberg-van Cittert, J.H.A., Visscher, H., 2001. Life in the end-Permian dead zone. Proc. Natl. Acad. Sci. 98, 7879–7883.

Malkowski, K., Gruszczynski, M., Hoffman, A., Halas, S., 1989. Oceanic stable isotope composition and a scenario for the Permo-Triassic crisis. Hist. Biol. 2, 289–309.

Marenco, P.J., Corsetti, F.A., Bottjer, D.J., Baud, A., Kaufman, A.J., 2005. Sulfur isotopic anomalies across the Permo-Triassic boundary and through the Early Triassic (abstract): International Symposium on Triassic Chronostratigraphy and Biotic Recovery, Chaohu, China. Albertiana 33, 57–58.

Maruoka, T., Koeberl, C., Hancox, P.J., Reimold, W.U., 2003. Sulfur geochemistry across a terrestrial Permian–Triassic boundary section in the Karoo Basin, South Africa. Earth Planet. Sci. Lett. 206, 101–117.

McManus, J.M., Berelson, W.M., Coale, K.H., Johnson, K.S., Kilgore, T.E., 1997. Phosphorus regeneration in continental margin sediments. Geochim. Cosmochim. Acta 61, 2891–2907.

Michaelsen, P., 2002. Mass extinction of peat-forming plants and the effect on fluvial styles across the Permian–Triassic boundary, northern Bowen Basin, Australia. Palaeogeogr. Palaeoclimatol. Palaeoecol. 179, 173–188.

Mossmann, J.-R., Aplin, A.C., Curtis, C.D., Coleman, M.L., 1991. Geochemistry of inorganic and organic sulphur in organic-rich sediments from the Peru Margin. Geochim. Cosmochim. Acta 55, 3581–3595.

Müller, R.D., Goncharov, A., Kritski, A., 2005. Geophysical evaluation of the enigmatic Bedout basement high, offshore northwestern Australia. Earth Planet. Sci. Lett. 237, 264–284.

Mundil, R., Ludwig, K.R., Metcalfe, I., Renne, P.R., 2004. Age and timing of the Permian mass extinctions: U/Pb dating of closed-system zircons. Science 305, 1760–1763.

Mundil, R., Metcalfe, I., Ludwig, K.R., Renne, P.R., Oberli, F., Nicoll, R.S., 2001. Timing of the Permian–Triassic biotic crisis: implications from new zircon U/Pb age data (and their limitations). Earth Planet. Sci. Lett. 187, 131–145.

Newell, A.J., Tverdokhlebov, V.P., Benton, M.J., 1999. Interplay of tectonics and climate on a transverse fluvial system, Upper Permian, Southern Uralian Foreland Basin, Russia. Sediment. Geol. 127, 11–29.

Newton, R.J., Pevitt, E.L., Wignall, P.B., Bottrell, S.H., 2004. Large shifts in the isotopic composition of seawater sulphate across the Permo-Triassic boundary in northern Italy. Earth Planet. Sci. Lett. 218, 331–345.

Nguyen, T.K.T., Dang, T.H., Ellwood, B.B., Lu, T.P.L., Doan, N.T., 2004. Determination of Permian–Triassic boundary in limestone formations from northeast of Vietnam by paleontological and MSEC methods. J. Sci. Earth 26, 222–232 (in Vietnamese with English abstract).

Nielsen, J.K., Shen, Y., 2004. Evidence for sulfidic deep water during the Late Permian in the East Greenland Basin. Geology 32, 1037–1040.

Payne, J.L., 2005. Evolutionary dynamics of gastropod size across the end-Permian extinction and through the Triassic recovery interval. Paleobiology 31, 269–290.

Payne, J.L., Lehrmann, D.J., Wei, J., Orchard, M.J., Schrag, D.P., Knoll, A.H., 2004. Large perturbations of the carbon cycle during recovery from the end-Permian extinction. Science 305, 506–509.

Payne, J.L., Lehrmann, D.J., Christensen, S., Wei, J., Knoll, A.H., 2006. Environmental and biotic controls on the initiation and growth of a Middle Triassic (Anisian) reef complex on the margin of the Great Bank of Guizhou, Guizhou Province, China. Palaios 21, 325–343.

Pruss, S.B., Bottjer, D.J., 2004. Late Early Triassic microbial reefs of the western United States: a description and model for their deposition in the aftermath of the end-Permian mass extinction. Palaeogeogr. Palaeoclimatol. Palaeoecol. 211, 127–137.

Rampino, M.R., Adler, A.C., 1998. Evidence for abrupt latest Permian mass extinction of Foraminifera; results of tests for the Signor–Lipps effect. Geology 26, 415–418.

Raup, D.M., 1979. Size of the Permo-Triassic bottleneck and its evolutionary implications. Science 206, 217–218.

Reichow, M.K., Al'Mukhamedov, A.I., Kirda, N.P., Medvedev, A.I., Pringle, M.S., Saunders, A.D., White, R.V., 2002. ^{40}Ar/^{39}Ar dates from the West Siberian Basin; Siberian flood basalt province doubled. Science 296, 1846–1849.

Renne, P.R., Basu, A.R., 1991. Rapid eruption of the Siberian Traps flood basalts at the Permo-Triassic boundary. Science 253, 176–179.

Renne, P.R., Zheng, Z.C., Richards, M.A., Black, M.T., Basu, A.R., 1995. Synchrony and causal relations between Permian–Triassic boundary crisis and Siberian flood volcanism. Science 269, 1413–1416.

Retallack, G.J., 1995. Permian–Triassic extinction on land. Science 267, 77–80.

Retallack, G.J., 2005. Earliest Triassic claystone breccias and soil-erosion crisis. J. Sediment. Res. 75, 679–695.

Retallack, G.J., Veevers, J.J., Morante, R., 1996. Global early Triassic coal gap between Permo-Triassic extinction and middle Triassic recovery of swamp floras. Geol. Soc. Amer. Bull. 108, 195–207.

Retallack, G.J., Seyedolali, A., Krull, E.S., Holser, W.T., Ambers, C.P., Kyte, F.T., 1998. Search for evidence of impact at the Permian–Triassic boundary in Antarctica and Australia. Geology 26, 979–982.

Retallack, G.J., Smith, R.M.H., Ward, P.D., 2003. Vertebrate extinction across Permian–Triassic boundary in Karoo Basin, South Africa. Geol. Soc. Amer. Bull. 115, 1133–1152.

Rhodes, M.C., Thayer, C.W., 1991. Mass extinctions: ecological selectivity and primary production. Geology 19, 877–880.

Ripley, E.M., Lightfoot, P.C., Li, C., Elswick, E.R., 2003. Sulfur isotope studies of continental flood basalts in the Noril'sk region: implications for the association between lavas and ore-bearing intrusions. Geochim. Cosmochim. Acta 67, 2805–2817.

Rodhe, H., 1992. Modeling biogeochemical cycles. In: Butcher, S.S., Charlson, R.J., Orians, G.H., Wolfe, G.V. (Eds.), Global Biogeochemical Cycles. Academic Press, London, pp. 55–72.

Ryskin, G., 2003. Methane-driven oceanic eruptions and mass extinctions. Geology 31, 741–744.

Sakai, H., Casadevall, T.J., Moore, J.G., 1982. Chemistry and isotope ratios of sulphur in basalts and volcanic gases at Kilauea volcano, Hawaii. Geochim. Cosmochim. Acta 46, 729–738.

Sakai, H., Des Marais, D.J., Ueda, A., Moore, J.G., 1984. Concentrations and isotope ratios of carbon, nitrogen and sulphur in ocean-floor basalts. Geochim. Cosmochim. Acta 48, 2433–2441.

Sano, H., Nakashima, K., 1997. Lowermost Triassic (Griesbachian) microbial bindstone–cementstone facies, Southwest Japan. Facies 36, 1–24.

Schubert, J.K., Bottjer, D.J., 1992. Early Triassic stromatolites as post-mass extinction disaster forms. Geology 20, 883–886.

Schubert, J.K., Bottjer, D.J., 1995. Aftermath of the Permian–Triassic mass extinction event: paleoecology of Lower Triassic carbonates in the western USA. Palaeogeogr. Palaeoclimatol. Palaeoecol. 116, 1–39.

Sephton, M.A., Veefkind, R.J., Looy, C.V., Visscher, H., Brinkhuis, H., de Leeuw, J.W., 2001. Lateral variations in end-Permian organic matter. In: Buffetaut, E., Koeberl, C. (Eds.), Geological and Biological Effects of Impact Events. Springer, Berlin, pp. 11–24.

Sephton, M.A., Brinkhuis, H., Looy, C.V., Veefkind, R.J., Visscher, H., de Leeuw, J.W., 2002. Synchronous record of δ^{13}C shifts in the oceans and atmosphere at the end of the Permian. In: Koeberl, C., MacLeod, K.G. (Eds.), Catastrophic Events and Mass Extinctions; Impacts and Beyond. Geol. Soc. Am. Spec. Paper, vol. 356, pp. 455–462.

Sephton, M.A., Looy, C., Brinkhuis, H., Wignall, P.B., de Leeuw, J.W., Visscher, H., 2005. Catastrophic soil erosion during the end-Permian biotic crisis. Geology 33, 941–944.

Sepkoski Jr., J.J., 1996. Patterns of Phanerozoic extinction: a perspective from global data bases. In: Walliser, O.H. (Ed.), Global Events and Event Stratigraphy in the Phanerozoic. Springer, Berlin, pp. 35–51.

Shao, L., Zhang, P., Dou, J., Shen, S., 2000. Carbon isotope compositions of the Late Permian carbonate rocks in southern China: their variations between the Wujiaping and Changxing formations. Palaeogeogr. Palaeoclimatol. Palaeoecol. 161, 179–192.

Sheldon, N.D., Retallack, G.J., 2002. Low oxygen levels in earliest Triassic soils. Geology 30, 919–922.

Shukla, A.D., Bhandari, N., Shukla, P.N., 2000. Permian–Triassic transitional environment in Spiti Valley, Himalayas, India (abstract). Proceedings of the Conference on Catastrophic Events and Mass Extinctions: Impacts and Beyond. Vienna, Austria, July 9–12, 2000.

Stanley, S.M., Yang, X., 1994. A double mass extinction at the end of the Paleozoic era. Science 266, 1340–1344.

Strauss, H., 1997. The isotopic composition of sedimentary sulfur through time. Palaeogeogr. Palaeoclimatol. Palaeoecol. 132, 97–118.

Suzuki, N., Ishida, K., Shinomiya, Y., Ishiga, H., 1998. High productivity in the earliest Triassic ocean: black shales, Southwest Japan. Palaeogeogr. Palaeoclimatol. Palaeoecol. 141, 53–65.

Swartzendruber, L.J., 1992. Properties, units and constants in magnetism. J. Magn. Magn. Mater. 100, 573–575.

Taylor, K.G., Macquaker, J.H.S., 2000. Spatial and temporal distribution of authigenic minerals in continental shelf sediments: implications for sequence stratigraphic analysis. In: Glenn, C.R., Prévôt-Lucas, L., Lucas, J. (Eds.), Marine Authigenesis: From Global to Microbial. SEPM (Soc. Sedim. Geol.) Spec. Publ., vol. 66. SEPM-SSG, Tulsa, Oklahoma, pp. 309–323.

Twitchett, R.J., 1999. Palaeoenvironments and faunal recovery after the end-Permian mass extinction. Palaeogeogr. Palaeoclimatol. Palaeoecol. 154, 27–37.

Twitchett, R.J., 2005. The Lilliput effect in the aftermath of the end-Permian extinction event. Albertiana 33, 79–81.

Twitchett, R.J., Looy, C.V., Morante, R., Visscher, H., Wignall, P.B., 2001. Rapid and synchronous collapse of marine and terrestrial ecosystems during the end-Permian biotic crisis. Geology 29, 351–354.

Twitchett, R.J., Krystyn, L., Baud, A., Wheeley, J.R., Richoz, S., 2004. Rapid marine recovery after the end-Permian mass-extinction event in the absence of marine anoxia. Geology 32, 805–808.

Vasconcelos, C., McKenzie, J.A., Warthmann, R., Bernasconi, S.M., 2005. Calibration of the δ^{18}O paleothermometer for dolomite precipitated in microbial cultures and natural environments. Geology 33, 317–320.

Visscher, H., Looy, C.V., Brinkhuis, H., Van Konijnenburg-Van Cittert, J.H.A., Kürschner, W.M., Collinson, M., Sephton, M.A.,

2004. Environmental mutagenesis at the time of the end Permian ecological crisis. Proc. Natl. Acad. Sci. 101, 12,952–12,956.

Walsh, M.M., Lowe, D.R., 1999. Modes of accumulation of carbonaceous matter in the early Archean; a petrographic and geochemical study of the carbonaceous cherts of the Swaziland Supergroup. In: Lowe, D.R. (Ed.), Geologic Evolution of the Barberton Greenstone Belt, South Africa. Geol. Soc. Am. Spec. Pap., vol. 329, pp. 115–132.

Wang, C.J., Visscher, H., 2007. Abundance anomaly of alkyldibenzofurans and alkylphenols in the marine sediments across PTB as indicators for end-Permian global terrestrial and marine ecosystem collapse based on the Meishan section, China. Palaeogeogr. Palaeoclimatol. Palaeoecol. 252, 281–290 (this volume). doi:10.1016/j.palaeo.2006.11.052.

Wang, K., Geldsetzer, H.H.J., Krouse, H.R., 1994. Permian–Triassic extinction: organic δ^{13}C evidence from British Columbia, Canada. Geology 22, 580–584.

Ward, P.D., 2000. Rivers in Time: The Search for Clues to Earth's Mass Extinctions. Columbia University Press, New York. 315 pp.

Ward, P.D., Montgomery, D.R., Smith, R., 2000. Altered river morphology in South Africa related to the Permian–Triassic extinction. Science 289, 1740–1743.

Watson, J.S., Sephton, M.A., Looy, C.V., Gilmour, I., 2005. Novel oxygen-containing aromatic compounds in Permian sediment. Org. Geochem. 36, 371–384.

Weidlich, O., Kiessling, W., Flügel, E., 2003. Permian–Triassic boundary interval as a model for forcing marine ecosystem collapse by long-term atmospheric oxygen drop. Geology 31, 961–964.

Wigley, T.M.L., Plummer, L.N., 1976. Mixing of carbonate waters. Geochim. Cosmochim. Acta 40, 989–995.

Wignall, P.B., Hallam, A., 1992. Anoxia as a cause of the Permian–Triassic extinction: facies evidence from northern Italy and the western United States. Palaeogeogr. Palaeoclimatol. Palaeoecol. 93, 21–46.

Wignall, P.B., Newton, R., 2003. Contrasting deep-water records from the Upper Permian and Lower Triassic of South Tibet and British Columbia: evidence for a diachronous mass extinction. Palaios 18, 153–167.

Wignall, P.B., Twitchett, R.J., 1996. Oceanic anoxia and the end Permian mass extinction. Science 272, 1155–1158.

Wignall, P.B., Twitchett, R.J., 2002. Extent, duration and nature of the Permian–Triassic superanoxic event. In: Koeberl, C., MacLeod, K.G. (Eds.), Catastrophic Events and Mass Extinctions: Impacts and Beyond. Geol. Soc. Am. Spec. Paper, vol. 356, pp. 395–413.

Wignall, P.B., Morante, R., Newton, R., 1998. The Permo-Triassic transition in Spitsbergen: $\delta^{13}C_{org}$ chemostratigraphy, Fe and S geochemistry, facies, fauna and trace fossils. Geol. Mag. 135, 47–62.

Wignall, P.B., Newton, R., Brookfield, M.E., 2005. Pyrite framboid evidence for oxygen-poor deposition during the Permian–Triassic crisis in Kashmir. Palaeogeogr. Palaeoclim. Palaeoecol. 216, 183–188.

Winguth, A.M.E., Maier-Reimer, E., 2005. Causes of marine productivity and oxygen changes associated with the Permian–Triassic boundary: a reevalution with ocean general circulation models. Mar. Geol. 217, 283–304.

Woods, A.D., Bottjer, D.J., 2000. Distribution of ammonoids in the Lower Triassic Union Wash Formation (eastern California): evidence for paleoceanographic conditions during recovery from the end-Permian mass extinction. Palaios 15, 535–545.

Woods, A.D., Bottjer, D.J., Mutti, M., Morrison, J., 1999. Lower Triassic large sea-floor carbonate cements: their origin and a mechanism for the prolonged biotic recovery from the end-Permian mass extinction. Geology 27, 645–648.

Xie, S., Pancost, R.D., Yin, H., Wang, H., Evershed, R.P., 2005. Two episodes of microbial change coupled with Permo/Triassic faunal mass extinction. Nature 434, 494–497.

Xu, D.-Y., Yan, Z., 1993. Carbon isotope and iridium event markers near the Permian–Triassic boundary in the Meishan section, Zhejiang Province, China. Palaeogeogr. Palaeoclimatol. Palaeoecol. 104, 171–176.

Yang, Z., Sheng, J., Yin, H., 1995. The Permian–Triassic boundary: the global stratotype section and point (GSSP). Episodes 18, 49–53.

Yin, H., Zhang, K., Tong, J., Yang, Z., Wu, S., 2001. The global stratotype section and point (GSSP) of the Permian–Triassic boundary. Episodes 24, 102–114.

Zhang, R., Follows, M.J., Grotzinger, J.P., Marshall, J., 2001. Could the Late Permian deep ocean have been anoxic? Paleoceanography 16, 317–329.